Lithos 320–321 (2018) 454–469

Contents lists available at ScienceDirect

Lithos

journal homepage: www.elsevier.com/locate/lithos

Metamorphic *P-T* path and SIMS zircon U-Pb dating of amphibolite of the Namche Barwa Complex, southeast Tibet, China

Tao Peng [a,b], Ling-Sen Zeng [c], Li-E Gao [c], Axel Gerdes [b], Jia-Hao Gao [c], Zhao-Ping Hu [c], Chun-Ming Wu [a,*]

[a] College of Earth and Planetary Sciences, University of Chinese Academy of Sciences, Beijing 100049, China
[b] Department of Geosciences, Goethe University Frankfurt, Frankfurt am Main 60438, Germany
[c] Institute of Geology, Chinese Academy of Geological Sciences, Beijing 100037, China

ARTICLE INFO

Article history:
Received 24 June 2018
Accepted 3 October 2018
Available online 6 October 2018

Keywords:
Amphibolite
Geothermobarometer
Namche Barwa Complex
SIMS U-Pb dating
P-T path
Tectonic exhumation

ABSTRACT

Amphibolite from the core and the outer part of the Namche Barwa Complex (NBC), southeast Tibet, experienced upper amphibolite facies metamorphism and records clockwise metamorphic *P-T* paths. Prograde (M1), peak (M2) and retrograde (M3) metamorphic mineral assemblages were identified in both amphibolite types. The M2 *P-T* conditions in the core and outer part of the NBC are similar: Zhibai amphibolite (ZBA, from the core), ~750 °C/10 kbar; Paixiang amphibolite (PXA, from the outer part), 670–750 °C/ 8.5–10.5 kbar. SIMS zircon U-Pb dating suggests that the protolith of PXA (the outer part of the NBC) formed at ~90–80 Ma, similar to the mafic dykes within the Tethyan Himalaya. This magmatism is probably related to tectonic events on the northern Indian passive margin before its collision with the Eurasian Plate. Furthermore, zircon records metamorphism from Oligocene to late Miocene (~30 Ma to ~10 Ma) in the ZBA, while PXA only documents a Miocene metamorphic event (~9 Ma). It is inferred that from Oligocene to late Miocene, semi-continuous advection of relatively hot material from the depth might have operated only in NBC core, thus exhuming the ZBA to a shallower level, while this material did not efficiently reach/affect the PXA. At late Miocene (~10 Ma) rapid exhumation started to propagate to the outer part of NBC and both units were amalgamated as a coherent block.

1. Introduction

The Namche Barwa Complex (NBC) exposed in southeast Tibet, China. As the eastern syntaxis of the Himalayan Orogenic Belt, the NBC has experienced a complex exhumation history closely related to the erosion of the deep Yarlu-Tsangpo gorge (Burg et al., 1997; Zeitler et al., 2001; Koons et al., 2013; Wang et al., 2014a, 2014b, 2014c). Conceptual models have suggested that the NBC experienced the intimated coupling of rapid erosion, high-grade metamorphism and partial melting (Zeitler et al., 2001 and 2014; Koons et al., 2013). Therefore, documenting its metamorphic evolution is critical for understanding the driving force behind these phenomena (Booth et al., 2009).

Exposed at the easternmost part of the Higher Himalayan Crystalline Sequence (HHCS), the NBC consists of diverse types of metamorphic rocks: metapelite, amphibolite, metagraywacke, ortho- or para-gneiss and migmatite (Sun et al., 2004; Geng et al., 2006; Zeng et al., 2012; Xu et al., 2012; Zhang et al., 2015; Tian et al., 2016). Previous studies show that the NBC experienced high-pressure (HP) granulite facies metamorphism (e.g. Liu and Zhong, 1997; Ding and Zhong, 1999). Reported metamorphic peak *P-T* conditions range from 11 to 18 kbar and 750 to 950 °C (Liu and Zhong, 1997; Ding and Zhong, 1999; Ding et al., 2001; Liu and Zhang, 2014; Booth et al., 2009; Guilmette et al., 2011; Zhang et al., 2015; Tian et al., 2016 and 2017). Dating of accessory phases points out metamorphic ages between 69 and 9 Ma (e.g. Ding et al., 2001; Liu and Zhang, 2014; Tian et al., 2016). The protracted and variable peak *P-T* conditions of the NBC metamorphic rocks have led to different tectonic models: (a) isothermal decompression (Liu and Zhong, 1997; Ding and Zhong, 1999; Ding et al., 2001; Booth et al., 2009); (b) decompression with cooling (Guilmette et al., 2011) and (c) decompression with heating followed by isothermal decompression (Zhang et al., 2015) or decompressional cooling (Tian et al., 2016). Such hypotheses are based mostly on petrological studies of mafic granulite lenses or other metamorphic rocks from the core of the NBC. Previous geological mapping shows that the NBC consists of at least of four tectonic slices (Bilu, Zhibai, Paixiang and Duoxiong-La) that differ in metamorphic grade and mineral assemblage (Geng et al., 2006; Burg et al., 1997 and 1998; Zeitler et al., 2001; Koons et al., 2013). Whether the metamorphic history unraveled from the core of the NBC is similar to that of other parts of the NBC, is still ambiguous and therefore deserves further investigation.

Amphibolite, as one of the important components in many orogenic belts, has been reported to be as early as Precambrian (e.g. de Gomes et al., 1964; Elueze, 1985; Vijaya Kumar et al., 2006; Xiao et al., 2013;

* Corresponding author.
E-mail address: wucm@ucas.ac.cn (C.-M. Wu).

https://doi.org/10.1016/j.lithos.2018.10.002
0024-4937/

Lu et al., 2014; Wang et al., 2014a, 2014b, 2014c; Chen et al., 2015; Meng et al., 2017), Paleozoic (e.g. Dupuy et al., 1979; Reimann and Stumpfl, 1985; Franceschelli et al., 2005; Peng et al., 2014; Wang et al., 2016a, b, 2017a, 2017b, 2018a, 2018b), Mesozoic (e.g. Bonini and Baldwin, 1998; Tsujimori et al., 2006; Marroni et al., 2014) to Cenozoic (e.g. Searle et al., 1992; Macfarlane, 1993; Coleman and Hodges, 1998; Cottle et al., 2009; Gao et al., 2013). Although amphibolite is not usually a representative rock of high temperature (HT) or high pressure (HP) metamorphic events, it still can provide key records on the tectono-metamorphic process of an orogenic belt. Because of stronger resistance to weathering, the chemical composition would not be altered as easily as metapelite. These properties make it a good recorder and accessible host for petrological investigation.

Amphibolite is more abundant than mafic granulite in different parts and structural levels of the NBC and provides an opportunity to compare the metamorphic *P-T* conditions and tectono-metamorphic evolution between both the Lower and Upper HHCS. Therefore, in this contribution, amphibolite samples were collected from different parts of the NBC to define their metamorphic history. The results help to distinguish the similarity and difference in metamorphic and tectonic history between the core and the outer part of the NBC.

2. Geological background

The Eastern Himalayan Syntaxis (EHS, Fig. 1), is located at the easternmost part of Himalayan Orogen, where the Indian Plate subducted beneath the Eurasian Plate, forming the "great 180-degree bend" of the Yarlung Tsangpo river. The NBC is the central part of EHS, and is mainly composed of metamorphic and granitic rocks of HHCS affinity. The Indus-Yarlung Tsangpo Suture Zone (IYSZ) occurs as an abruptly curved tectonic boundary between the Lhasa terrane and the NBC, and it is characterized by dismembered ophiolite and mélange (Xu et al., 2012). Furthermore, IYSZ can be divided into two sub-tectonic systems around the NBC: (a) the NE–SW striking, sinistral, strike-slip Dongjiu-Milin shear zone (DMSZ) in the west and (b) the dextral, strike-slip Aniqiao-Motuo shear zone (AMSZ) in the east (Burg et al., 1998; Xu Z.Q. et al., 2012). The Tethyan Himalayan Sequences (THS), consisting of Paleozoic to Mesozoic sedimentary strata, metamorphosed under greenschist to epidote-amphibolite facies (e.g. Booth et al., 2004, 2009; Liu et al., 2011), was considered to have been involved in the IYSZ or ubiquitously mylonitized in the shear zone (Ding et al., 2001; Xu et al., 2012). Thus, it is difficult to identify the accurate trending of the Southern Tibetan Detachment (STD) in this area.

The rocks in the NBC were originally named as the Namche Barwa Group by Zheng and Chang (1979). After updated field mapping, Sun et al. (2004) divided this group into three packages: (a) Zhibai formation (Zhibai Slice in Fig. 1), consisting of garnet-bearing gneiss with sporadic boudins of mafic granulite, garnet clinopyroxenite, kyanite-bearing pelitic granulite and garnet amphibolite; (b) Paixiang formation (Bilu and Qingqing-La Slice in Fig. 1), dominantly consisting of felsic gneiss with subordinate diopside and forsterite-bearing marble, clinopyroxenite and scapolite diopsidite and (c) Duoxiong-La

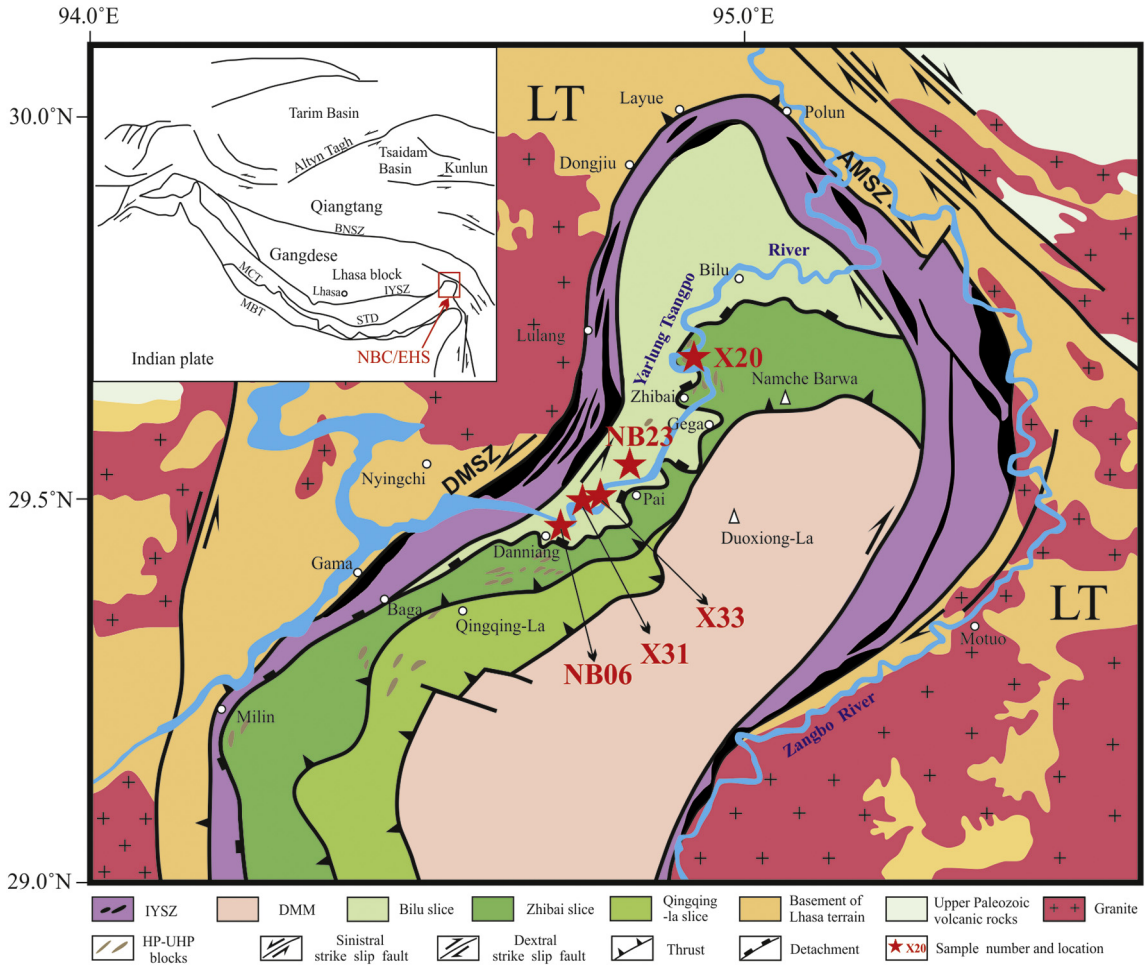

Fig. 1. Geological sketch map of the Namche Barwa Complex (NBC) and Eastern Himalaya Syntaxis (EHS). (Modified after Geng et al., 2006 and Xu Z.Q. et al., 2012). The pentagons represent the sample locations. MBT, the Main Boundary Thrust; MCT, the Main Central Thrust; STD, the South Tibetan Detachment; BNSZ, the Bangong-Nujiang Suture Zone; IYSZ, the Indus-Yarlung Tsangpo suture zone; DMSZ, the Dongjiu-Milin shear zone; AMSZ, the Aniqiao-Motuo shear zone; LZ: Basement of the Lhasa Terrane. Zhibai formation includes Zhibai Slice. Paixiang Formation includes Bilu and Qingqing-La slices.

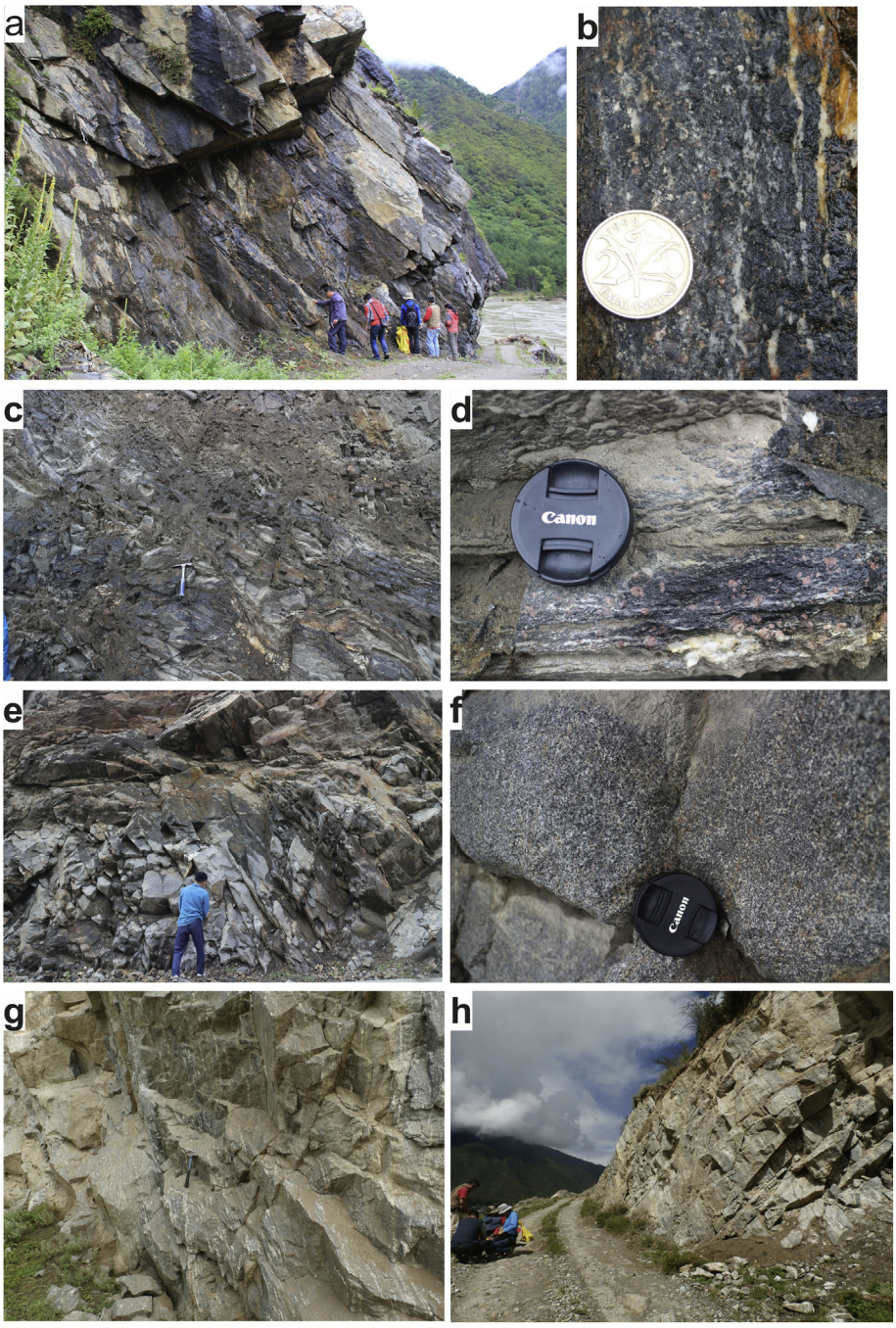

Fig. 2. Outcrops of the garnet-bearing amphibolite in the NBC. (a) and (b), sample X20, located in the Zhibai formation with leucovein; (c) and (d), sample NB06; (e) and (f), sample NB23; (g), sample X31 and (h), sample X33.

migmatite (DMM in Fig. 1), consisting of migmatitic gneiss, augen gneiss and banded gneiss, and outcropping over a large area in the eastern part of the NBC (Geng et al., 2006). Granitic gneiss, with Paleoproterozoic to Paleozoic protolith ages, within the NBC, indicates that this complex experienced pre-Himalayan magmatic events (e.g. Sun et al., 2005; Zhang et al., 2008; Guo et al., 2008; Zhang et al., 2012; Wang et al., 2014a, b, c). Despite of various pre-Himalayan tectonic events, different rock types of Namche Barwa commonly involved in the Cenozoic metamorphism up to granulite facies (Zhong and Ding, 1995; Liu and Zhong, 1997). The metamorphism was firstly considered to have occurred at about 45–69 Ma (Ding and Zhong; 1999). Ding et al. (2001) further constrained this event to be ~40 Ma. More recent studies show that nearly all types of rocks (i.e. mafic and pelitic granulite, amphibolite and metapelite) in the NBC record the ~25 Ma or ~18–20 Ma metamorphism (e.g. Xu et al., 2010; Zeng et al., 2012; Su et al., 2012; Liu and Zhang; 2014) and a retrograde, amphibolite-facies metamorphism at ~9 Ma (Liu and Zhang; 2014). Younger ages of ~10–0.8 Ma

Table 1
The P-T calculation results from thermobarometer.

	M1	M2		M3	
X20	No data obtained	749 °C, 10.0 kbar	GHPQ	624 °C, 3.5 kbar	Hbl-PT
X33	No data obtained	765 °C, 8.9 kbar	GHPQ	661 °C, 4.9 kbar	Hbl-PT
		757 °C, 9.8 kbar	GBPQ		
NB06	No data obtained	669 °C, 9.7 kbar	GHPQ	603 °C, 4.6 kbar	Hbl-PT
NB23	No data obtained	748 °C, 10.5 kbar	GHPQ	632 °C, 5.5 kbar	Hbl-PT
X31	No data obtained	785 °C, 10.3 kbar	GHPQ	No data obtained	
		675 °C, 9.7 kbar	GBPQ		

were also reported (Booth et al., 2009; Wang et al., 2014a, b, c). These retrograde metamorphic events may be related to the rapid exhumation of the NBC. Zhang et al. (2010) found that the High Himalayan rocks in the NBC experienced only high-*P* granulite-facies metamorphic event at 37–32 Ma, which needs further investigation.

3. Petrography

The amphibolite samples of this study were collected from Jiala (Zhibai formation), Danniang and Paixiang (Paixiang formation). Sample localities are shown in Fig. 1. At outcrop scale (Fig. 2a-b), amphibolite from the Zhibai slice (ZBA), core part of the NBC, exhibits remnants of a garnet-bearing mafic rock with lathy leucosome crystallized between melanosome, which probably formed as regional leucogranite during partial melting in the NBC (Zeng et al., 2012). The amphibolite from Paixiang formation (PXA), outer part of the NBC, occurs as either enclave or interlayer (Fig. 2c-h) within the metasedimentary rocks, with relatively less amounts of leucosome. From the metamorphic *P-T* paths and ages of these two types of amphibolite from different parts of the NBC, the tectono-metamorphic evolution of the NBC can be deciphered more comprehensively.

All the amphibolite samples exhibit similar matrix mineral assemblages, but differ in matrix mineral sizes and the composition of minerals in symplectites. In the following petrographic description, the abbreviations M1, M2 and M3 (including mineral subscript 1, 2, 3) refer to the sequential prograde, peak and retrograde stages of a metamorphic episode and the mineral abbreviations are after Whitney and Evans (2010).

3.1. Namche Barwa core (ZBA-sample X20: garnet amphibolite)

Sample X20 (29°40′52"N, 94°54′32″E) was collected at the foothill of Namche Barwa close to the Yarlung-Tsangpo river. This rock shows a massive structure and porphyroblastic texture. The porphyroblasts (10%) are relative uniform 1–3 mm sized garnet, which mainly includes Qz_1, Pl_1, Ttn_1, Ilm_1, Ap_1 and Zrn_1 as inclusions preserved in the core. The matrix, peak metamorphic assemblage consists of Grt_2, Hbl_2 (60%), Pl_2 (20%), Qz_2 (5%) and accessory minerals such as Ttn_2, Zrn_2 and Ap_2 (5%). The "white-eye socket" symplectite (Ma and Wang, 1994) surrounding Grt_2 porphyroblast, consists mainly of thin intergrowth of Hbl_3, Pl_3 and Qz_3.

The inclusion assemblage preserved in the garnet are ascribed to the prograde assemblage (M1) and mainly consists of tiny minerals Ttn_1 + Ilm_1 + Qtz_1 + Pl_1, while the matrix minerals – Grt_2, Hbl_2, Pl_2, Qz_2 and Zrn_2 constitute the metamorphic peak assemblage (M2). The symplectic assemblage of worm-like Hbl_3, Pl_3 and Qz_3 intergrowth is the retrograde assemblage (M3). The possible reactions responsible for the transformation of M1, M2 and M3 assemblages are:

$Ttn_1 + Ilm_1 + Pl_1 + (Hbl_1?) \rightarrow Grt_2 + Hbl_2 + Pl_2 + Ttn_2 \rightarrow Hbl_3 + Pl_3$.

3.2. Outer part of Namche Barwa(PXA)

3.2.1. Sample X31: garnet-bearing biotite-amphibolite gneiss

Sample X31 (29°27′47"N, 94°48′27″E) was collected from the north bank of the Yarlung-Tsangpo river, 3 km away from Paixiang. The rock shows gneissic structure and porphyroblastic texture. The porphyroblast is mainly garnet (5%), usually <2 mm in diameter and without inclusions. The garnet is usually rimmed by well preserved "white-eye socket" symplectite consisting of stick-like biotite, plagioclase and quartz intergrowth. The matrix assemblage includes granular Pl_2 (40%), short prismatic Hbl_2 (20%), flaky Bt_2 (15%), fine-grained Qz_2 (15%) and some of accessory minerals (e.g. Mag_2, Zrn_2) (5%). Only the metamorphic peak assemblage (M2) and retrograde assemblage (M3) are preserved. Transformation of the M3 from the M2 assemblages might follow this reaction:

$Grt_2 + Pl_2 + Hbl_2 + Bt_2 \rightarrow Bt_3 + Pl_3$.

3.2.2. Sample X33: garnet-bearing amphibolite

Sample X33 (29°27′46"N, 94°48′31″E) was collected 100 m to the east of sample X31, close to Paixiang. The rock also shows gneissic structure and porphyroblastic texture. Garnet (4%) is the major porphyroblast with size ranging from 1 to 3 mm, without inclusions. Grt_2 is rimmed by "white-eye socket" symplectite consisting of Hbl_3, Pl_3, Bt_3 and Qz_3 intergrowth (M3). The matrix mineral assemblage (M2) includes Hbl_2 (40%), Pl_2 (30%), Qz_2 (15%), Bt_2 (8%) and a small amount of Mag_2 and Zr_2 (3%). Similarly, transformation from M2 to M3 assemblages might follow the reaction:

$Grt_2 + Hbl_2 + Bt_2 + Pl_2 \rightarrow Hbl_3 + Bt_3 + Pl_3$.

3.2.3. Sample NB06: garnet-bearing amphibolite

Sample NB06 (29°27′48.54"N, 94°45′5.57″E) was collected near Danniang, on the east side of the Yarlung-Tsangpo river. The rock shows gneissic structure and porphyroblastic texture. Garnet (5%) is the main porphyroblast with diameters around 1 mm and tiny accessory minerals preserved as inclusions. Three generations of mineral assemblages have been identified. The prograde M1 assemblage consists of Pl_1 + Qtz_1 + Ap_1 + Rt_1 + Ttn_1 + Ilm_1 as mineral inclusions preserved in the garnet (M2). The metamorphic peak assemblage (M2) is composed of matrix minerals, i.e., Hbl_2 (50%), Pl_2 (20%), Qz_2 (20%), Grt_2 (5%), plus minor minerals Ilm_2, Ttn_2, Mag_2 and Zr_2. The retrograde assemblage (M3) is characterized by symplectite consisting of worm-like Hbl_3 + Pl_3 + Qz_3 intergrowth, rimming the garnet. The following metamorphic reactions are possibly responsible for the transformation from M1 to M2 and then to M3 assemblages:

$Rt_1 + Ttn_1 + Ilm_1 + Pl_1 + (Hbl_1?) \rightarrow Grt_2 + Hbl_2 + Ttn_1 + Ilm_1 + Pl_2 \rightarrow Hbl_3 + Pl_3$.

3.2.4. Sample NB23: garnet-bearing biotite amphibolite

Sample NB23 (29°31′16.44"N, 94°51′57.14″E) was sampled on the opposite bank of Paixiang, north side of the Yarlung-Tsangpo river. The structure and texture are similar to sample NB06, but with coarser biotite and different symplectic minerals. Garnet porphyroblasts are relatively small (diameter < 1 mm) and without inclusions. And two generations of mineral assemblages were observed. The metamorphic peak assemblage (M2) consists of Hbl_2, Bt_2, Pl_2, Grt_2 and Qz_2 in the matrix, as well as accessory minerals Mnz_2, Ilm_2, Ap_2 and Zr_2. Tiny irregular patchy Bt_3 and Pl_3 of the symplectite represents the retrograde mineral assemblage (M3). The possible metamorphic reaction from the M2 to M3 assemblages might be as follows:

$Grt_2 + Hbl_2 + Pl_2 \rightarrow Bt_3 + Pl_3$.

4. Mineral chemistry

Chemical compositions of the representative minerals of all the amphibolite samples were analyzed on the JOELSEM JXA 8230 electron microprobe at the School of Resources and Environmental Engineering, Hefei University of Technology, China. The analytical conditions were 15 kV accelerating voltage, a beam current of 20 nA with an electron beam size of 5 μm and 10–20 s counting time. Standards were natural minerals. The program ZAF was used for matrix corrections. Smaller mineral inclusions were analyzed using a 3 μm electron beam. Representative mean chemical compositions of the minerals are presented in Supplementary Table S1 and the estimated *P-T* conditions are listed in Table 1. Compositional features of the minerals are summarized below.

4.1. Garnet

X-ray compositional analysis was conducted on samples X20 and X33, and rim-core-rim compositional profiles (dashed red line with arrow in Fig. 3 a-e) were analyzed on the garnet porphyroblast for all

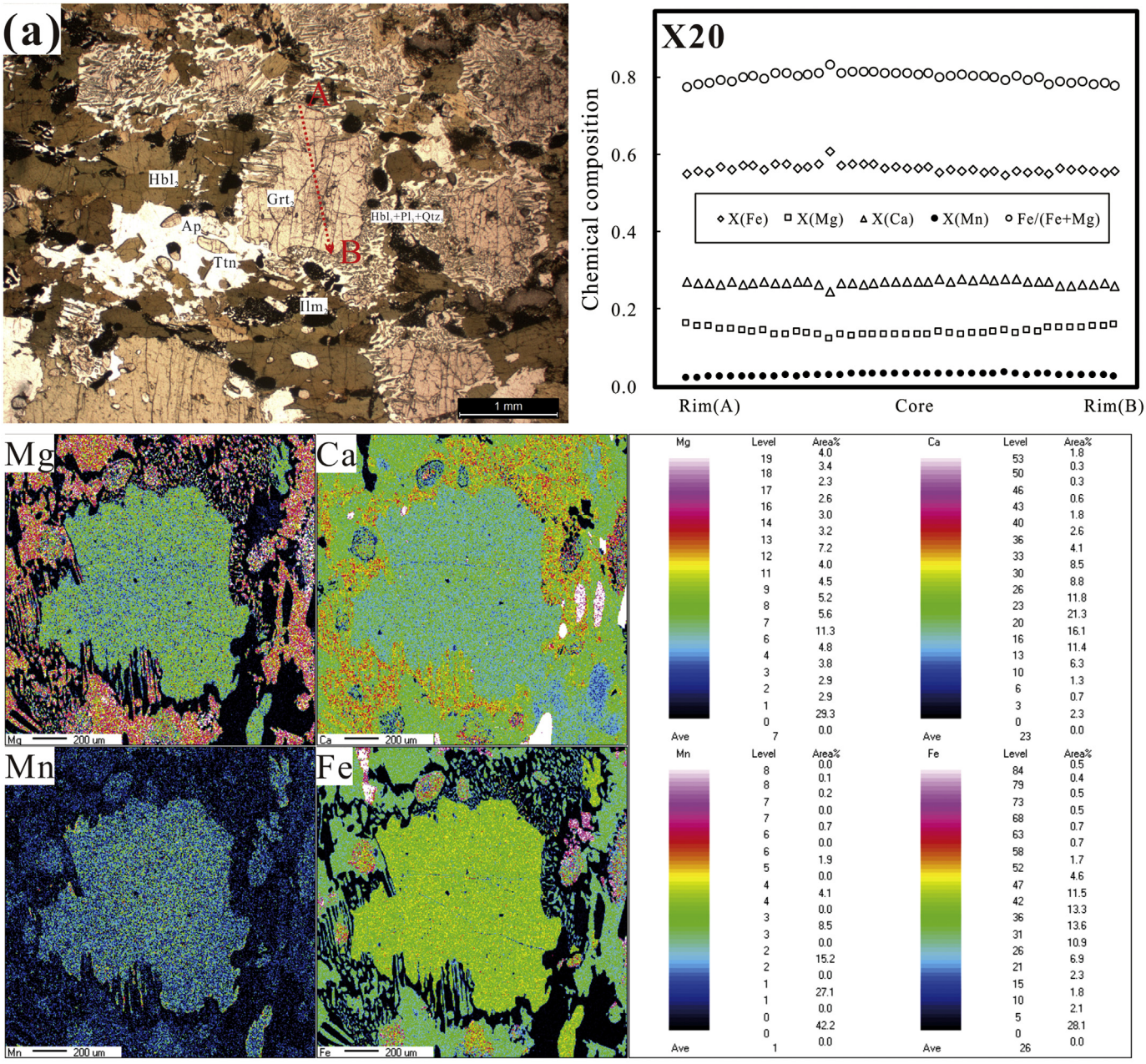

Fig. 3. Micropetrography of amphibolite in the NBC. (a) and (e) are micropetrographs, garnet profile and X-ray scanned compositional map of garnet of samples X20 and X30, respectively; (b), (c) and (d) are micropetrographs and garnet profiles of samples NB06, NB23 and X31, respectively.

the samples. Garnet is dominated by almandine, grossular with minor pyrope, and quite minor spessartine components. In samples X20 and NB06 the garnet has well preserved inclusions (M1). The elemental distribution profiles of the garnet indicate negligible chemical zoning from the core to the rim in all the samples.

4.2. Plagioclase

Plagioclase is present in the inclusion (Pl_1), matrix (Pl_2) and symplectic (Pl_3) assemblages. As Pl_1 is usually too small (1–2 μm) to be measured, only Pl_2 and Pl_3 were analyzed. Pl_2 is chemically homogeneous and is andesine (An = 30–46), whereas Pl_3 is Ca-rich plagioclase. Pl_3 in samples X23, X31 and X33 is labradorite (An = 50–69) whereas Pl_3 in samples X20 and NB06 are more Ca-richer (An = 70–86), attributed to bytownite. The higher Ca content of Pl_3 is related to its formation by the breakdown of the neighboring matrix garnet and hornblende.

4.3. Hornblende

Hornblende occurs as both matrix (Hbl_2) and symplectic (Hbl_3) minerals in samples X20, X33, NB06 and NB23, and only appears in the matrix (Hbl_2) in samples X05 and X31. No measurable hornblende inclusions were found in these samples. In samples X20 and NB23, Al_2O_3 content increases from Hbl_2 to Hbl_3 (12.5 to 10.6 wt%, 15.7 to 14.3%, respectively). The TiO_2 component also exhibits slight decrease from Hbl_2 to Hbl_3. All hornblende crystals contain similar CaO (9.7–11.4 wt%) and low Na_2O (1.5–2.2 wt%) components (Table S1) and are classified as calcic amphibole.

4.4. Biotite

Biotite is present both in the matrix (Bt_2) and symplectic (Bt_3) assemblages in sample X31, but only appears in the matrix (Bt_2) in sample

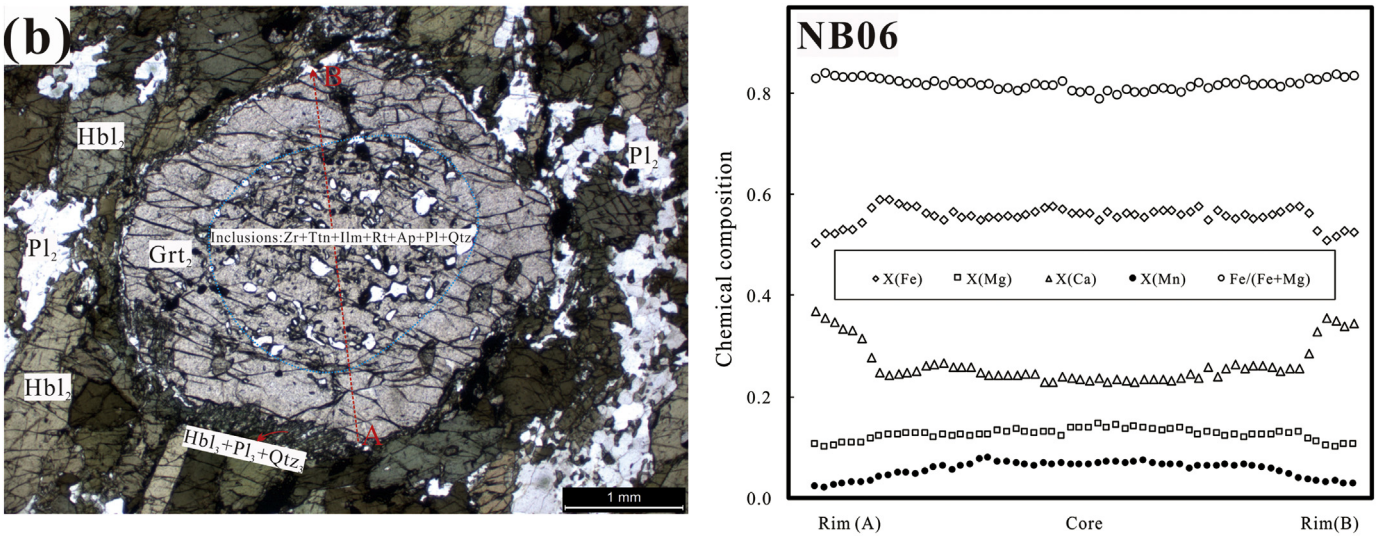

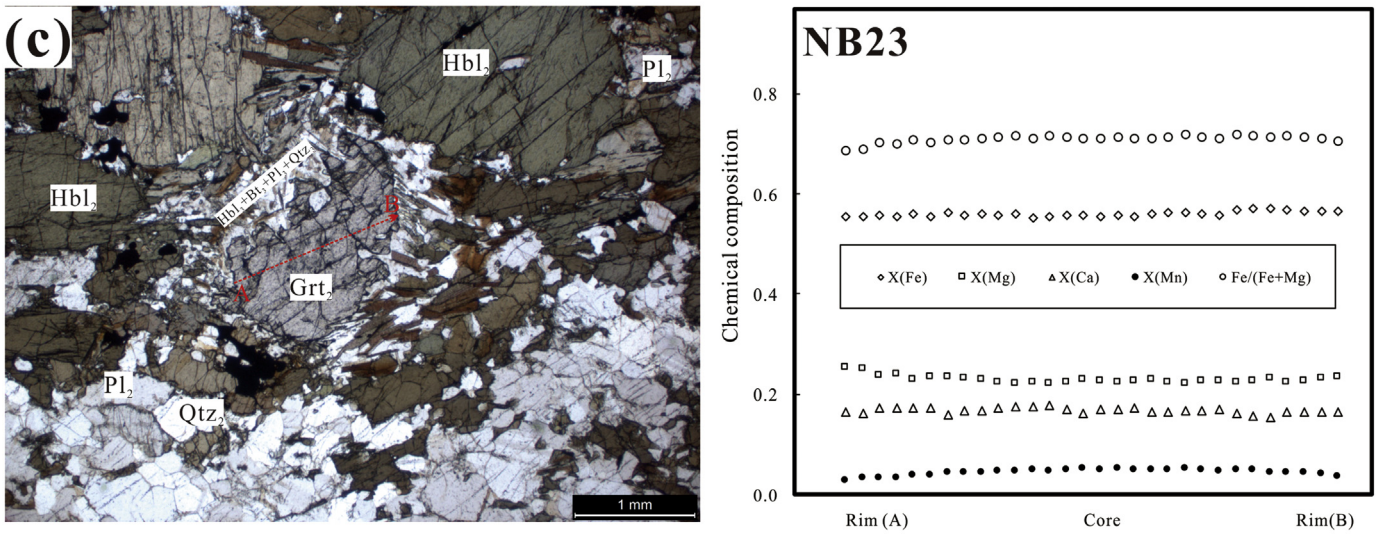

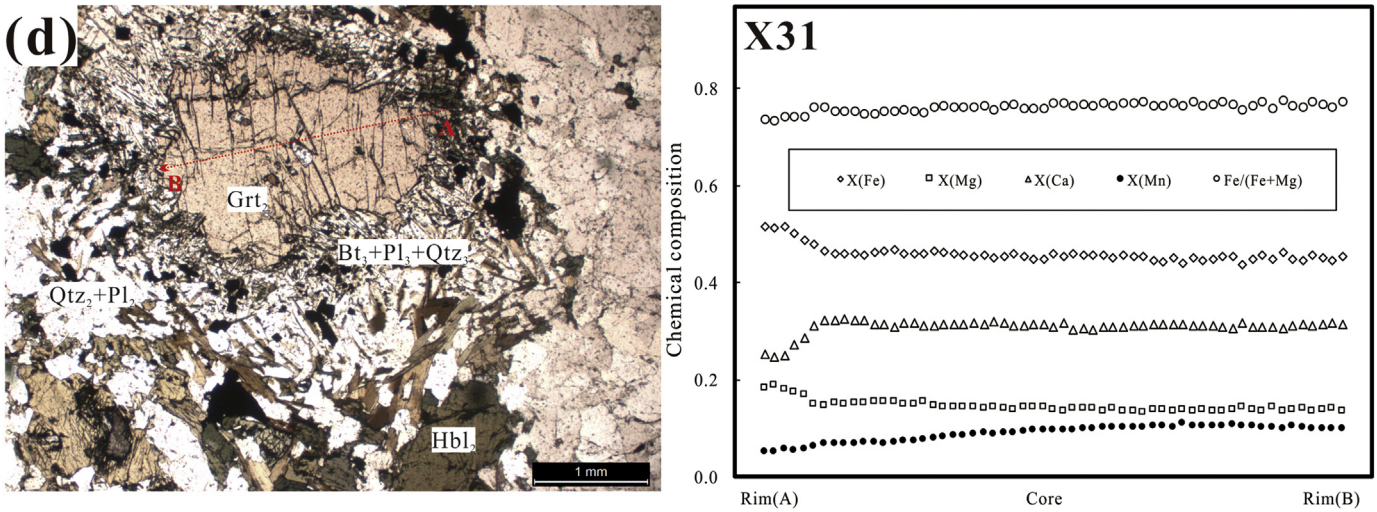

Fig. 3 (*continued*).

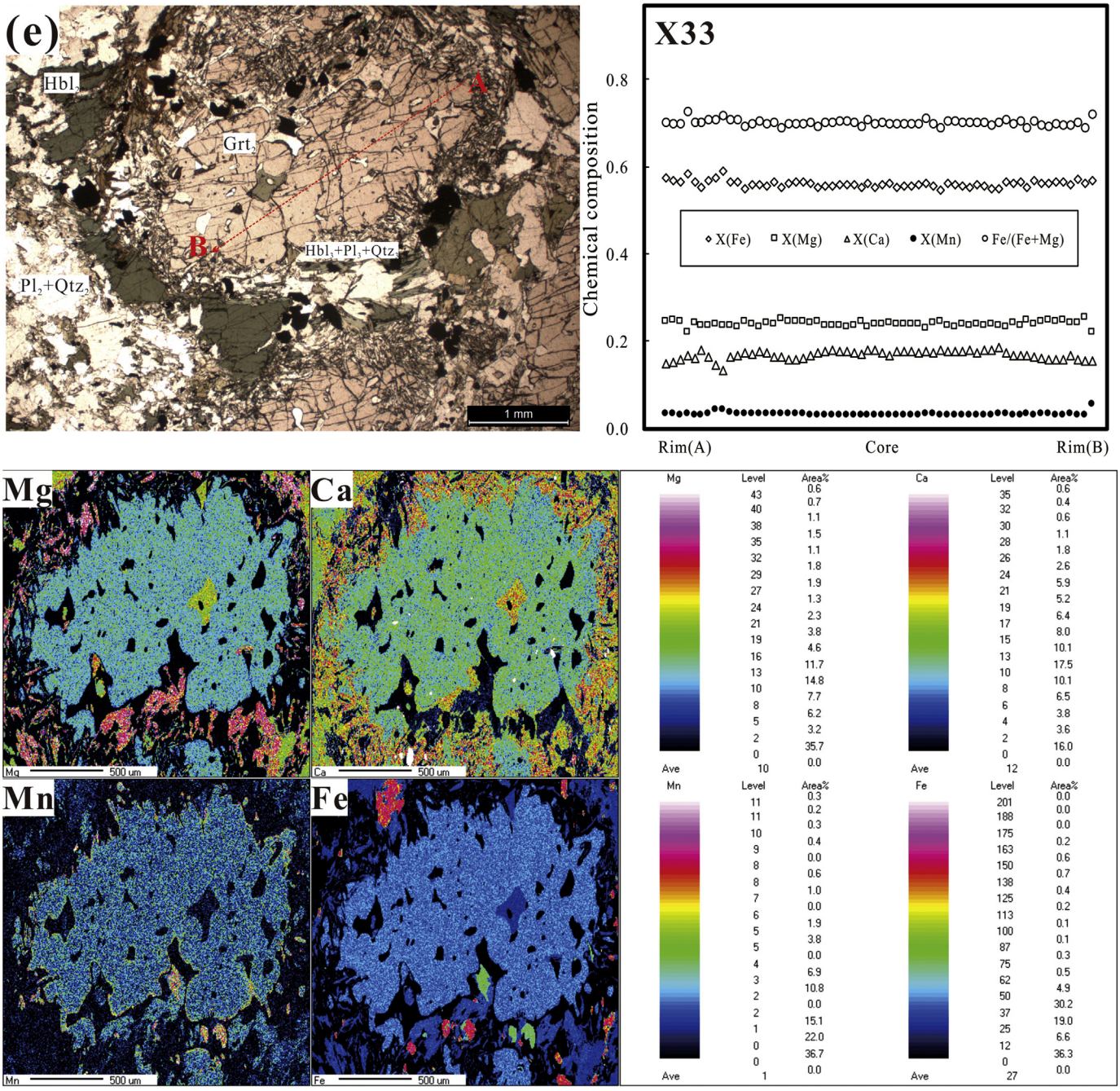

Fig. 3 (*continued*).

X33, and only appears in the symplectite (Bt_3) in sample NB23. In sample X31, the Bt_2 has a higher TiO_2 (3.7 wt%) and K_2O (9.2 wt%) components than Bt_3 (2.5 and 8.5 wt%, respectively).

5. Metamorphic *P-T* paths

The lack of appropriate mineral inclusions impedes the analyses and thus the estimation of *P-T* conditions for the prograde mineral assemblages (M1). For the metamorphic peak assemblage (M2) the *P-T* conditions were simultaneously determined by applying the garnet-hornblende-plagioclase-quartz (GHPQ) geobarometer (Dale et al., 2000) coupled with the hornblende-plagioclase thermometer (Holland and Blundy, 1994), as well as the garnet-biotite thermometer (Holdaway, 2000) together with the garnet-biotite-plagioclase-quartz (GBPQ) geobarometer (Wu et al., 2004). The estimated random errors of the GHPQ and the GBPQ geothermobarometers are ±40 °C / ± 1.1 kbar and ± 25 °C / ± 1.2 kbar, respectively. To determine the M2 *P-T* conditions, the near-rim composition of garnet was adopted. As for the retrograde assemblage (M3), only the single-hornblende thermobarometer (Gerya et al., 1997), whose random errors are ±37 °C and ± 1.2 kbar, is applicable. This is because of the high Ca content in Pl_3 exceeding the applicable chemical composition of plagioclase for the plagioclase-related geothermobarometers (e.g. Holland and Blundy, 1994; Bhadra and Bhattacharya, 2007). The *P-T* results are listed in Table 1.

The metamorphic peak (M2) and retrograde (M3) *P-T* conditions of ~750 °C / 10 kbar and ~625 °C / 3.5 kbar were retrieved for sample X20 of the Zhibai formation at the core part of the NBC. Similar *P-T* conditions of the samples, collected from the outer part of the NBC, were obtained: ~670–790 °C / 8.5–10.5 kbar (M2) and ~600–660 °C / 4.5–

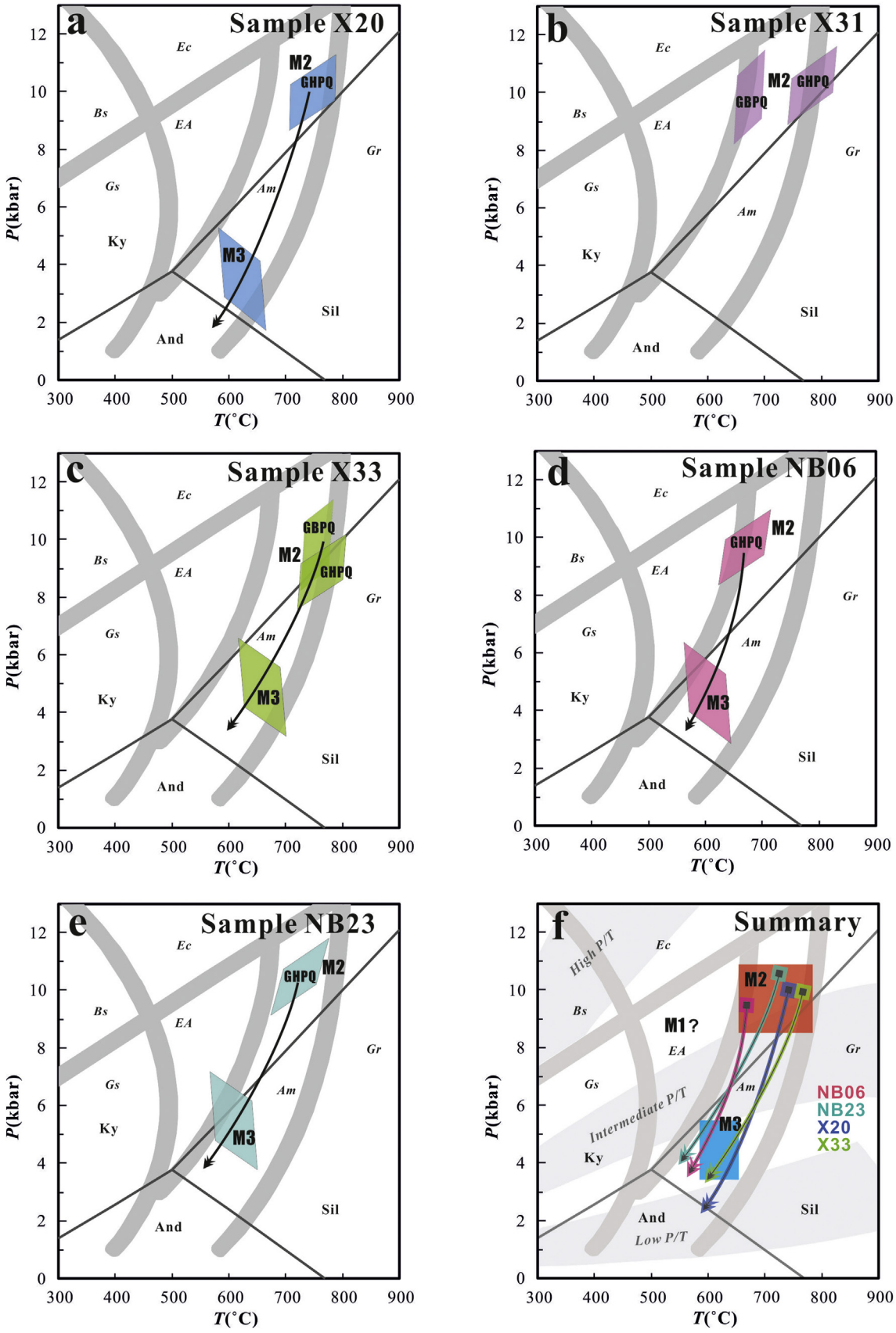

Fig. 4. Metamorphic *P-T* conditions and *P-T* paths of the NBC amphibolite. See text for explanation of geothermobarometry. Rhombuses are metamorphic *P-T* conditions considering random error of thermobarometers. (a) to (e) are metamorphic *P-T* conditions or *P-T* paths of samples X20, X31, X33, NB06 and NB23, respectively. (f) is the summary of all the *P-T* paths. Metamorphic facies and metamorphic facies series are from O'Brien and Rötzler (2003) and Spear (1993), respectively. The Al_2SiO_5 polymorph transition lines are from Holdaway and Mukhopadhyay (1993).

Table 2
SIMS U-Pb geochronological data of zircon extracted from amphibolite samples X20, X31 &X33. Analytical data with asterisk * were not used for computation in U-Pb concordia diagrams. The f_{206} is the proportion of the non-radiogenic ^{206}Pb of the total ^{206}Pb.

Spots	U(ppm)	Th(ppm)	Pb(ppm)	Th/U	f_{206}(%)	$\frac{207_{Pb}}{235_U}$	±σ (%)	$\frac{206_{Pb}}{238_U}$	±σ (%)	$\frac{206_{Pb}}{238_U}$	Age ± σ (Ma)
a. Qinghu standard											
Qinghu@1	2558	1691	81	0.661	0.12	0.1730	1.6	0.02529	1.5	161.0	2.4
Qinghu@2	2774	1113	82	0.401	0.02	0.1725	2.3	0.02523	2.2	160.6	3.5
Qinghu@3	1731	675	52	0.390	0.00	0.1718	1.7	0.02542	1.5	161.8	2.4
Qinghu@4	621	217	18	0.349	0.08	0.1676	2.2	0.02455	1.5	156.3	2.3
Qinghu@5	1798	876	53	0.487	0.05	0.1699	1.8	0.02487	1.5	158.4	2.4
Qinghu@6	1601	701	47	0.438	0.09	0.1697	1.8	0.02494	1.5	158.8	2.4
Qinghu@7	1890	897	57	0.475	0.04	0.1704	1.7	0.02519	1.5	160.4	2.4
b. Sample results (Only for the older group with age > 80 Ma of X31 and X33, a ^{204}Pb-based common Pb correction has been applied)											
X31@01	860	433	15	0.503	0.19	0.09247	2.7	0.01406	1.6	90.0	1.4
X31@03	905	394	16	0.436	0.00	0.09566	2.0	0.01438	1.5	92.0	1.4
X31@04	1163	754	21	0.648	0.06	0.09489	2.1	0.01441	1.5	92.3	1.4
X31@05	414	192	7	0.464	0.29	0.09193	3.6	0.01404	1.6	89.9	1.4
X31@06	640	469	12	0.734	0.33	0.09494	2.2	0.01425	1.5	91.2	1.4
X31@07	359	297	6	0.828	0.28	0.08924	3.7	0.01377	1.6	88.2	1.4
X31@08*	200	150	3	0.747	0.00	0.09078	3.3	0.01340	1.5	85.8	1.3
X31@10*	237	172	4	0.727	0.43	0.08805	3.8	0.01357	1.6	86.9	1.3
X31@11*	286	209	5	0.732	0.00	0.08595	3.0	0.01318	1.6	84.4	1.3
X31@12	391	163	7	0.417	0.31	0.09553	3.2	0.01430	1.5	91.5	1.4
X31@15	91	44	2	0.478	0.49	0.09161	4.6	0.01427	1.7	91.3	1.6
X31@17	316	148	6	0.469	0.00	0.09385	2.8	0.01452	1.6	92.9	1.4
X31@18	310	155	5	0.500	0.23	0.09199	2.8	0.01412	1.6	90.4	1.4
X31@20*	576	84	9	0.146	25.96	0.07901	56.1	0.01417	3.3	90.7	3.0
X33@01	262	24	4	0.090	0.14	0.08733	4.3	0.01293	1.8	82.8	1.5
X33@02	289	186	5	0.643	0.27	0.09211	4.6	0.01394	1.8	89.2	1.6
X33@03	719	34	10	0.047	0.21	0.08601	3.1	0.01313	1.5	84.1	1.3
X33@05*	205	13	3	0.063	0.00	0.08366	4.5	0.01249	1.8	80.0	1.4
X33@06*	297	49	4	0.166	1.07	0.07351	10.5	0.01300	1.6	83.2	1.4
X33@08	1232	73	18	0.060	0.15	0.09000	2.4	0.01380	1.5	88.3	1.4
X33@09	641	48	9	0.075	0.23	0.08801	2.9	0.01324	1.6	84.8	1.3
X33@11	295	31	4	0.105	0.59	0.08650	3.3	0.01372	1.6	87.8	1.4
X33@13*	384	1	5	0.003	0.28	0.07977	3.4	0.01259	1.6	80.7	1.3
X33@14*	368	18	5	0.048	0.18	0.08382	3.1	0.01275	1.6	81.6	1.3
X33@15	317	15	5	0.049	0.83	0.09106	3.2	0.01346	1.5	86.2	1.3
X33@16*	355	34	5	0.095	0.69	0.08359	3.3	0.01326	1.6	84.9	1.3
X33@17	152	16	2	0.103	0.83	0.08614	4.3	0.01297	1.6	83.1	1.3
X33@20	837	82	12	0.098	0.00	0.09121	2.3	0.01345	1.5	86.1	1.3
X33@21	380	53	6	0.140	0.37	0.08925	2.9	0.01330	1.5	85.2	1.3
X33@22	509	52	8	0.103	0.15	0.08971	3.0	0.01363	1.6	87.3	1.3
X33@23	372	17	5	0.044	0.58	0.08898	3.0	0.01313	1.6	84.0	1.4
c. Sample results (All adopted 207-corr Age)											
X20@1	41	6	0	0.150	2.86	215.6	3.1	0.04957	10.1	29.7	0.9
X20@2	51	7	0	0.137	0.00	290.3	3.1	0.04341	12.7	22.3	0.7
X20@3	166	25	1	0.151	0.00	353.8	2.2	0.04359	7.1	18.3	0.4
X20@4	32	8	0	0.260	26.31	391.1	4.6	0.19980	9.0	13.2	0.7
X20@5	125	2	1	0.018	0.59	244.1	2.8	0.04705	6.3	26.3	0.7
X20@6	93	25	0	0.265	29.27	400.1	4.1	0.15389	9.4	13.9	0.7
X20@7	81	13	0	0.166	0.00	437.5	5.3	0.06255	13.3	14.4	0.8
X20@8	27	8	0	0.300	31.08	255.1	5.0	0.05730	18.5	24.9	1.3
X20@9	66	11	0	0.172	16.81	261.8	3.6	0.10598	13.7	22.8	0.9
X20@10	23	7	0	0.303	30.50	564.9	9.1	0.11204	26.4	10.4	1.0
X20@11	97	3	0	0.029	7.61	260.7	2.7	0.05494	9.6	24.4	0.7
X20@12	98	13	0	0.132	0.00	355.5	3.2	0.05201	11.5	18.0	0.6
X20@13	246	73	1	0.295	0.92	388.3	2.8	0.04808	12.0	16.5	0.5
X20@14	41	9	0	0.212	3.53	253.2	4.2	0.05523	16.0	25.1	1.1
X20@15	53	10	0	0.185	9.36	292.7	3.3	0.05571	13.7	21.7	0.7
X20@16	16	3	0	0.205	42.90	558.7	10.5	0.09340	28.1	10.8	1.2
X20@17	199	44	0	0.222	5.12	429.3	3.0	0.04397	11.5	15.0	0.5
X20@18	80	25	0	0.307	10.81	301.3	3.0	0.05246	11.2	21.2	0.7
X20@19	89	26	0	0.294	9.69	426.7	4.5	0.05423	12.6	14.9	0.7
X20@20	86	16	0	0.191	16.64	428.0	4.0	0.08377	14.6	14.3	0.6
X20@21	47	0	0	0.004	3.22	163.1	3.0	0.04868	11.3	39.3	1.2
X20@22	38	1	0	0.036	10.95	179.6	5.3	0.06175	11.7	35.1	1.9
X20@23*	87	13	0	0.145	10.91	366.7	4.6	0.04512	12.6	17.6	0.8
X31@1	860	433	15	0.503	0.19	71.01	1.6	0.04918	1.6	90.0	1.4
X31@2	44	1	0	0.021	0.00	715.7	6.2	0.07503	16.5	8.8	0.6
X31@3	905	394	16	0.436	0.00	69.55	1.5	0.04825	1.4	92.0	1.4
X31@4	1163	754	21	0.648	0.06	69.34	1.5	0.04825	1.2	92.3	1.4
X31@5	414	192	7	0.464	0.29	71.02	1.5	0.04974	2.2	89.9	1.4
X31@6	640	469	12	0.734	0.33	70.17	1.5	0.04832	1.6	91.2	1.4
X31@7	359	297	6	0.828	0.28	72.40	1.6	0.04918	2.2	88.3	1.4
X31@8*	200	150	3	0.747	0.00	74.63	1.5	0.04914	2.9	85.7	1.3
X31@9	41	1	0	0.019	16.39	690.2	6.0	0.04502	21.1	9.5	0.6
X31@10*	237	172	4	0.727	0.43	73.71	1.6	0.04707	3.5	86.9	1.4

Table 2 (*continued*)

Spots	U(ppm)	Th(ppm)	Pb(ppm)	Th/U	f_{206}(%)	$\frac{207_{Pb}}{235_U}$	±σ (%)	$\frac{206_{Pb}}{238_U}$	±σ (%)	$\frac{206_{Pb}}{238_U}$	Age ± σ (Ma)
X31@11*	286	209	5	0.732	0.00	75.89	1.6	0.04731	2.5	84.4	1.4
X31@12	391	163	7	0.417	0.31	69.93	1.5	0.04845	2.8	91.5	1.4
X31@13	60	2	0	0.031	6.67	694.0	5.1	0.04657	18.1	9.4	0.5
X31@14	68	2	0	0.025	36.27	781.4	7.1	0.05764	15.9	8.2	0.6
X31@15	91	44	2	0.478	0.49	70.09	1.7	0.04657	4.3	91.5	1.6
X31@16	20	1	0	0.041	43.51	610.7	7.8	0.06750	22.8	10.4	0.8
X31@17	316	148	6	0.469	0.00	68.89	1.6	0.04689	2.3	93.0	1.4
X31@18	310	155	5	0.500	0.23	70.83	1.6	0.04726	2.4	90.4	1.4
X31@19*	108	81	2	0.752	0.00	84.32	1.8	0.04971	4.2	75.8	1.4
X31@20*	576	84	9	0.146	25.96	52.26	2.7	0.24687	4.5	91.3	3.6
X31@21	32	0	0	0.003	31.92	654.2	7.3	0.05857	29.0	9.8	0.7
X31@22*	87	0	0	0.004	13.44	677.6	6.9	0.04578	13.1	9.6	0.7
X33@1	262	24	4	0.090	0.14	77.24	1.8	0.05013	3.1	82.7	1.5
X33@2	289	186	5	0.643	0.27	71.56	1.8	0.05005	3.0	89.2	1.6
X33@3	719	34	10	0.047	0.21	76.02	1.5	0.04919	1.9	84.1	1.3
X33@4*	556	45	7	0.081	0.30	82.20	2.2	0.04926	2.2	77.8	1.7
X33@5*	205	13	3	0.063	0.00	80.03	1.8	0.04856	4.1	80.0	1.4
X33@6*	297	49	4	0.166	1.07	76.11	1.6	0.04953	3.8	83.9	1.4
X33@7	164	2	0	0.009	7.92	720.9	3.8	0.05915	11.0	8.9	0.3
X33@8	1232	73	18	0.060	0.15	72.48	1.5	0.04731	1.9	88.4	1.4
X33@9	641	48	9	0.075	0.23	75.52	1.5	0.04820	2.4	84.7	1.3
X33@10	131	2	0	0.018	5.73	717.3	5.3	0.05196	19.6	9.0	0.5
X33@11	295	31	4	0.105	0.59	72.88	1.6	0.04572	2.9	88.1	1.4
X33@12	141	2	0	0.016	6.97	667.7	5.5	0.04737	13.0	9.7	0.5
X33@13*	384	1	5	0.003	0.28	79.40	1.6	0.04593	3.1	80.9	1.3
X33@14*	368	18	5	0.048	0.18	78.45	1.6	0.04769	2.6	81.6	1.3
X33@15	317	15	5	0.049	0.83	74.28	1.5	0.04906	2.8	86.1	1.3
X33@16*	355	34	5	0.095	0.69	75.41	1.6	0.04572	2.9	85.1	1.3
X33@17	152	16	2	0.103	0.83	77.10	1.6	0.04816	4.0	83.0	1.4
X33@18	68	0	0	0.002	29.14	596.1	7.3	0.06701	16.4	10.6	0.8
X33@19*	59	0	no data	0.001	4.35	563.9	4.7	0.05603	16.1	11.4	0.5
X33@20	837	82	12	0.098	0.00	74.38	1.5	0.04920	1.7	85.9	1.3
X33@21	380	53	6	0.140	0.37	75.20	1.5	0.04868	2.5	85.1	1.3
X33@22	509	52	8	0.103	0.15	73.34	1.6	0.04772	2.6	87.3	1.4
X33@23	372	17	5	0.044	0.58	76.28	1.6	0.04923	2.5	83.8	1.4

5.5 kbar (M3), respectively. Therefore, the amphibolite in the NBC might have experienced similar metamorphic evolution, although it is outcropping in different parts of the NBC.

The metamorphic peak (M2) *P-T* conditions belong to the amphibolite facies and the medium *P/T* facies series. Four samples (X20, X33, NB06 and NB23) record clockwise *P-T* paths (Fig. 4). The *P-T* paths from the peak (M2) to retrograde (M3) stages indicates a decompression and cooling process, possibly indicating a relatively quick tectonic exhumation after the amphibolite reached the maximum depth. However, similar *P-T* paths do not necessarily relate to the same metamorphic event, as will be discussed in the next section.

6. SIMS U-Pb dating of zircon

6.1. Method

Zircon grains separated from the amphibolite samples X20, X31 and X33 were vacuum-coated with high-purity gold prior to SIMS analysis, and isotopes of U, Th, and Pb were measured using a Cameca IMS-1280 SIMS mass spectrometer at the Institute of Geology and Geophysics, Chinese Academy of Sciences (IGGCAS), Beijing. Detailed descriptions of the instrument and analytical procedure are given in Li et al. (2009). The size of the primary O_2^- ion beam spot is set as ~30 μm × 20 μm. Reference zircon Plešovice ($^{206}Pb/^{238}U$ age = 337.13 ± 0.37 Ma, Sláma et al., 2008) was used to calibrate Pb/U ratio and reference zircon 91,500 (Th = 29 ppm, and U = 81 ppm, Wiedenbeck et al., 1995) was adopted to calibrate the U and Th concentration. The measured Pb content was corrected for common Pb using non-radiogenic ^{204}Pb and in case of young zircon the ^{207}Pb-based common Pb correction method has been applied. An average present-day crustal composition (Stacey and Kramers, 1975) was adopted for common Pb based on the assumption that the common Pb is largely related to surface contamination introduced during sample preparation. The Isoplot/Ex v. 4.15 program (Ludwig, 2012) was used for data reduction. Uncertainties on individual analyses in the data table (Table 2) are reported at 1σ level, and the concordia U/Pb (Pb/Pb) mean ages are given at the 95% confidence level. To monitor the external uncertainties of SIMS U-Pb zircon dating, an in-house zircon standard Qinghu was alternately analyzed as an unknown together with other unknown zircon grains. Seven measurements on Qinghu zircon (Table 2a) yielded a concordia age of 159.6 ± 1.9 Ma (Fig. 6a), which is identical within error with the recommended value of 159.5 ± 0.2 Ma (Li et al., 2013). A long-term uncertainty of 1.5% (1σ RSD) for $^{206}Pb/^{238}U$ measurements of the standard zircons was propagated to the unknowns (Li et al., 2010), despite that the measured $^{206}Pb/^{238}U$ error in a specific session is generally ≤1% (1σ RSD). The analytical data are listed in Table 2.

Due to its high precision on young zircon (<500 Ma), the $^{206}Pb/^{238}U$ ages are used for interpretation. Low U and thus ^{206}Pb contents in Cenozoic zircon, with common Pb correction using ^{204}Pb, can result in imprecise or even incorrect U-Pb ages (Li et al., 2012; Yang et al., 2014). The $^{206}Pb/^{238}U$ age using the ^{207}Pb common Pb correction (207-Corr age) assuming concordancy generally is more reliable for younger zircons. Some data are excluded because the possible mixture of two different domains of the zircon or they are outliers in comparison to others.

6.2. Analytical results

Three samples were dated in this study and the results of SIMS analyses are listed in Table 2b and c. The spot locations are shown on CL images in Fig. 5.

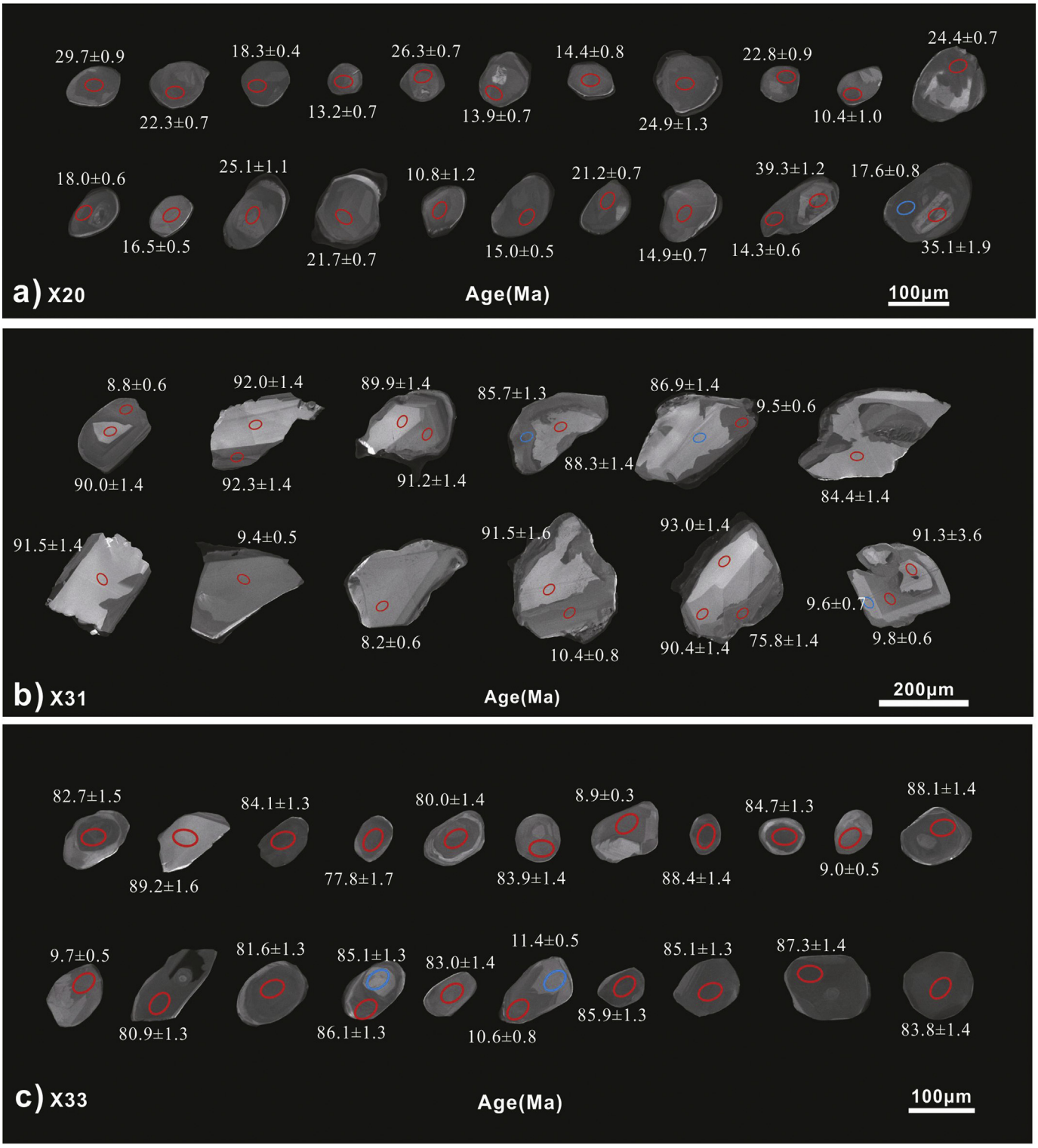

Fig. 5. Representative cathodoluminescence (CL) images of zircon of amphibolite of the NBC. The ellipse represents analytical spot locations for secondary ion mass spectrometry (SIMS). Numbers adjacent to the zircon are ^{207}Pb common Pb-corrected ages. Some spots also obtain the $^{206}Pb/^{238}U$ age corrected by ^{204}Pb, which are very close or identical to 207-corrected ages. The isotope data are shown in Table 2b. Data points shown in blue ellipses are excluded from age calculation, because their isotope composition may possibly be contaminated by adjacent previous measured spots. These data are shown with asterisk in Table 2.

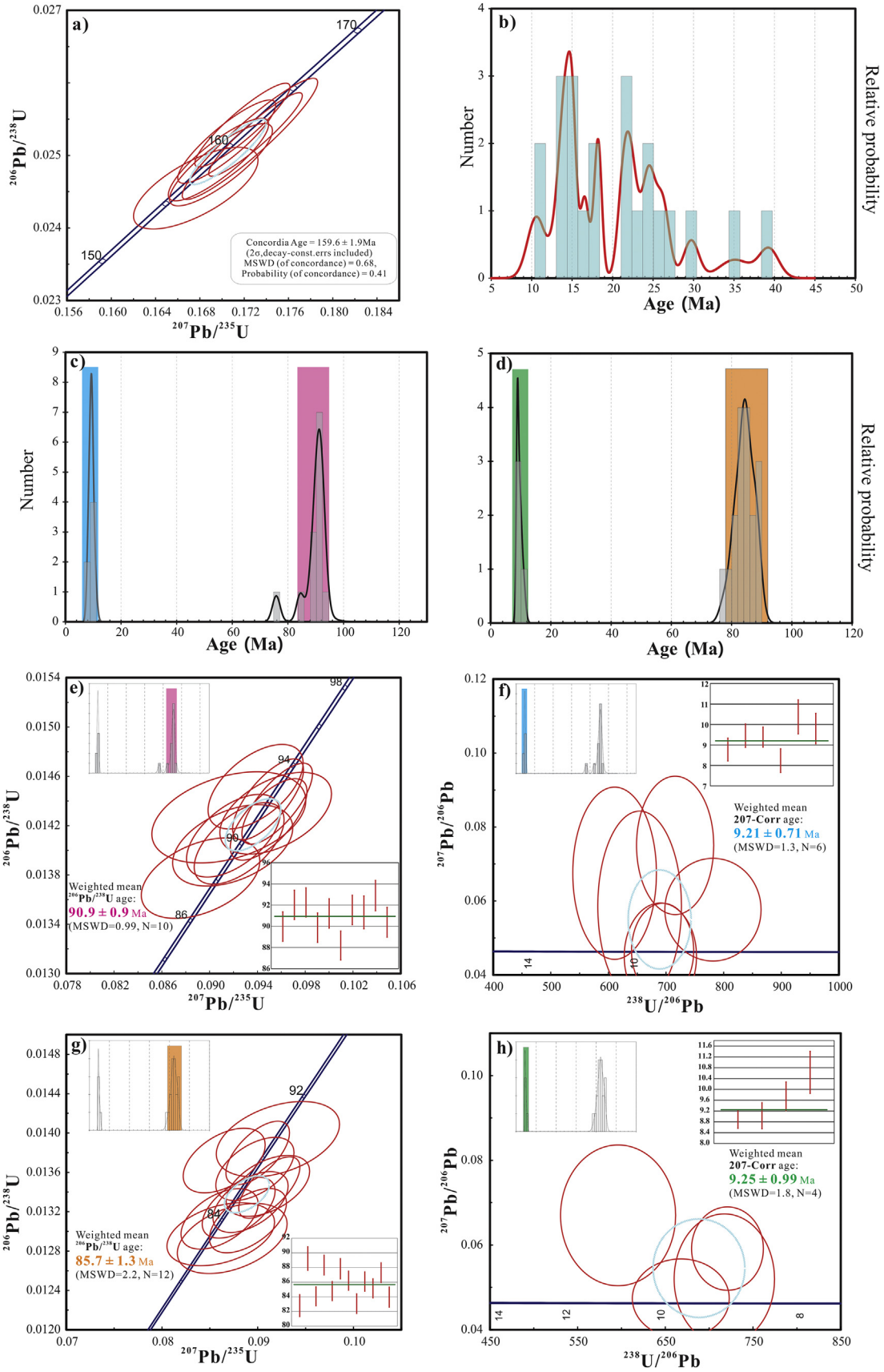

Fig. 6. Concordia diagram for SIMS U-Pb analysis. (a) Concordia diagram for zircon standard Qinghu. (b-d) Probability density diagrams for zircon ages of samples X20, X31 and X33, respectively. The colored shades mark the two main age groups. Sample X20 data show continuous zircon (re-)crystallization during metamorphism from ~30 Ma to ~10 Ma, whereas samples X31 and X33 are characterized by a huge gap between ~80 Ma and ~9 Ma. (e) and (g) Concordia diagram for older zircon age group of samples X31 and X33; (f) and (h) Tera-Wasserburg diagram for younger age group of samples X31 and X33.

Zircon grains separated from sample X20 are 40 to 130 μm long and well-rounded with patchy or homogenous texture (Fig. 5a) in the wide outer domains, whereas the cores show distinct oscillatory zoning. Overall they resemble the characteristics described of high-grade metamorphic zircon (Hoskin and Black, 2000; Corfu et al., 2003; Hoskin and Schaltegger, 2003). Three types of overgrowth structures, core-mantle-rim, core-rim and homogeneous (Fig. 5a), were observed in these zircon grains. For those with inherited cores, the core shows relics of broad oscillatory zoning, as it is typical from magmatic zircon. Therefore, the ages of such cores possibly represent the protolith ages. Zircon grains which both rim and mantle are homogeneous in CL, indicating (re-) crystallization during metamorphism. Many zircon grains show a distinct narrow (<5 μm) dark rim, which is too small to conduct meaningful analysis. Thus, ages were only obtained from core and mantle. We have performed a total of 23 analyses on 21 zircon grains. Two measurements on oscillatory zoning yielded ages of 39.3 ± 1.2 Ma and 35.1 ± 1.9 Ma, possibly indicating Eocene magmatism. The remaining spot analyses yielded ages (Fig. 6b) from ~30 Ma to ~10 Ma, with a gap at ~21–18 Ma. It is noteworthy to point out that among these measured zircon grains, the mantle in the youngest two grains yielded age of ~10 Ma, suggesting that the dark narrow outermost rim is younger than ~10 Ma.

Zircon grains in sample X31 show similar overgrowth texture to those in sample X20, although they are much larger by a factor of 2–4. We performed 22 spot analyses on 12 zircon grains. Except for several spots which possibly yielded mixed ages of the core and mantle, the cores yielded substantially older ages than the metamorphic rim. The core and mantle yielded ages between ~84 and ~93 Ma and among which ten spots yielded a weighted $^{206}Pb/^{238}U$ ages of 90.9 ± 0.9 Ma ($N = 10$, MSWD = 0.99) (Fig. 6e), with higher Th/U (> 0.4). This age is interpreted to date the formation of its protolith. Zircon rims are characterized by much younger ages ranging from 10.4 to 8.2 Ma with a weighted mean 207-Corr age of 9.21 ± 0.71 Ma ($N = 6$, MSWD = 1.3) (Fig. 6f), which is interpreted to represent the metamorphic age.

For sample X33, most of its zircon grains are ovoid to round in shape and are <100 μm long. Unlike the previous samples, there are no obvious core-mantle-rim structures in these zircon grains. We performed 23 spot analyses on 21 grains (Table 2b and c). Those with broad growth zoning yielded ages older than 80 Ma and are characterized by moderate to high U (152–1232 ppm) but low Th (mostly <80 ppm) contents and thus low Th/U ratios (< 0.1). These spots yielded a $^{206}Pb/^{238}U$ age of 85.7 ± 1.3 Ma ($N = 12$, MSWD = 2.2) (Fig. 6g), slightly younger than that of sample X31. Analysis on the brighter and homogeneous CL domains of those grains are characterized by moderate U (59–164 ppm) but low Th (< 2 ppm) contents, resulting also in low Th/U ratios (<0.1). The obtained ages range from ~8 Ma to ~11 Ma. Four spots yielded a weighted mean 207-Corr age of 9.25 ± 0.99 Ma ($N = 4$, MSWD = 1.8, Fig. 6h), and is interpreted to represent the metamorphic age.

7. Discussion

7.1. Metamorphic history and tectonic implication

Since Zhong and Ding (1995) first reported HP granulite in the NBC, many studies (e.g. Liu and Zhong, 1997; Ding et al., 2001; Booth et al., 2009; Zhang et al., 2015; Liu and Zhang, 2014; Tian et al., 2016) have been carried out to constrain the metamorphic *P-T* conditions in the Zhibai formation. Previous studies have shown that the estimated metamorphic peak *P-T* conditions range from 10 to 18 kbar and 700 to 950 °C. The wide *P-T* interval might be due to the following reasons: (1) different methods were used in determining the *P-T* conditions of different rocks; or (2) the rocks really record different metamorphic *P-T* conditions of varied tectonic levels. Our amphibolite samples are from different parts of the NBC and their metamorphic peak *P-T* conditions (ZBA, ~750 °C/10 kbar; PXA, 670–750 °C/ 8.5–10.5 kbar) are similar, which possibly implies that the ZBA and PXA once reached similar depth. As the amphibolite samples are interlayered with / enclosed in the metasedimentary rocks, it can be inferred that the PXA, from the outer part of the NBC, together with its surrounding metasedimentary rocks, were once carried to depths comparable with those reached by the ZBA in the NBC core. However, it is unclear whether the ZBA and PXA have experienced such similar peak metamorphism simultaneously.

The HP granulite facies metamorphism in the NBC was previously considered to have occurred at ~40 Ma (Ding et al., 2001), with retrograde stage occurred at 18–23 Ma. Further studies interpreted U-Pb zircon ages of ~20–25 Ma as recording the HP metamorphic stage (e.g. Xu et al., 2013; Liu and Zhang, 2014; Tian et al., 2016) and ~9 Ma as the retrograde stage (Liu and Zhang, 2014). Much younger ages (< 10 Ma) have also been reported, e.g. monazite U-Th-Pb and titanite U-Pb ages of ~3–10 Ma (Booth et al. 2009), zircon U-Th-He, apatite and zircon fission track, and biotite $^{40}Ar/^{39}Ar$ cooling ages of <10 Ma (Wang et al., 2014a, b, c), and zircon U-Pb age from 0.8 to 10 Ma (Zeitler et al., 2014). Based on low Th/U ratios (<0.1) of their analyses, Zeitler et al. (2014) interpreted that these young ages are related to the zircon growth during the tectonic exhumation (decompression) coupled with fluid infiltration and/or partial melting (e.g. Rubatto, 2002). Such tectonic exhumation process might have occurred also in the amphibolite of the NBC, albeit no evidences show that our samples once reached granulite facies condition.

The zircon from the ZBA (X20) yielded U-Pb ages from ~30 Ma to 10 Ma, which are nearly identical to recently reported zircon ages (29.2–10.2 Ma) from amphibolite in the NBC core (Tian et al., 2017). Such age pattern might be due to: (i) zircon only records two events and incomplete resetting during the second event caused the dispersed ages; or (ii) zircon grew with fluid infiltration, at different but continuous episodes of metamorphism. As the ZBA contains leucosome veins, it possibly suggests the existence of fluid for zircon growth. Therefore, the interpretation of more than two metamorphic episodes reported in previous studies (e.g. Ding et al., 2001; Xu et al., 2010; Zeng et al., 2012; Su et al., 2012; Liu and Zhang 2014) seems more plausible. Two samples (X31 and X33) of the PXA only record the main metamorphic event during late Miocene (~11 Ma to ~8 Ma). The younger ages, especially for those of late Miocene from the zircon rim with very low Th/U ratio (<0.1, Fig. 7), are interpreted as metamorphic ages (e.g., Hoskin and Schaltegger, 2003; Schulz et al., 2006; Yakymchuk et al., 2018). In addition, some outermost rim of the zircon grains, which is too narrow to perform analysis, should record ages possibly younger than 10 Ma. It is noteworthy that all these amphibolite samples contain leucosome veins at the outcrop scale, which might play an important role in the overgrowth of zircon grains.

Protracted high-*T* metamorphism can be explained when considering semi-continuous advection of relatively hot material from depth (Koons et al., 2013; Zeitler et al., 2001), which could promote partial melting by decompression and heating up of those rocks at relatively shallower levels. It should be noted that the zircon ages from the ZBA indicate a continuous metamorphic event (~30 Ma to ~10 Ma), while those from the PXA only record metamorphic ages younger than ~9 Ma. It can be inferred that since Oligocene, such advection process might have operated only in the NBC core, thus exhumed the ZBA to a shallower level with continuous dissolution and overgrowth of zircon grains. Whereas zircon grains in the PXA could not grow because of lacking of fluids until ~10 Ma. Previous study, on mineral cooling ages (<10 Ma, Wang et al., 2014a, b, c) from the upstream of the Yarlung-Tsangpo river, suggests that both the NBC core and the outer part have undergone similar exhumation process since ~10 Ma. The age differences in the amphibolite from the core and the outer part of the NBC might suggest a rim-ward progressive exhumation, i.e., the NBC experienced rapid exhumation initiated from the core before ~10 Ma, and then propagated to the outer part of the NBC at ~10 Ma, and finally, they were amalgamated as a coherent block.

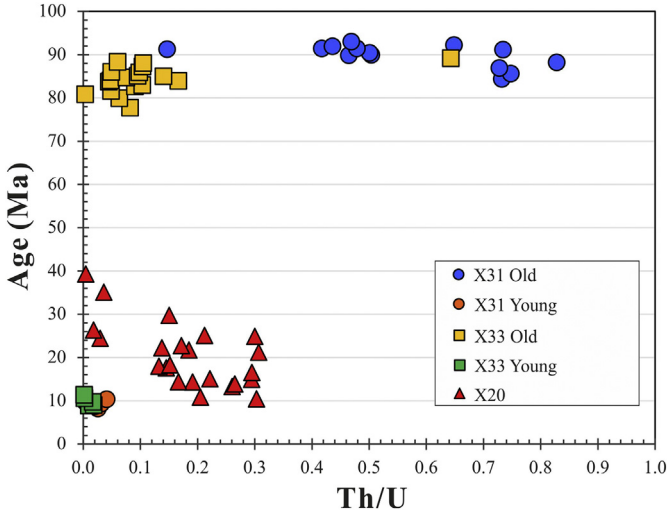

Fig. 7. Plot of ^{207}Pb common Pb-corrected age versus Th/U ratio for zircon of samples X20, X31 and X33. Most zircon grains, especially the younger population at ~9 Ma, has Th/U ratios <0.1, except for older population of X31 zircon (Th/U = 0.4–0.9).

7.2. Late Cretaceous magmatism

Zircon cores from the PXA samples X31 and X33 record similar ages of ~80–90 Ma, but with distinct Th/U ratios (X31, Th/U < 0.2; X33, Th/U = 0.4–0.9; Fig. 7). The tight age cluster and relict oscillatory zoning of the zircon are consistent with the idea that they record the protolith age. In fact, the mafic rocks with similar crystallization ages have been reported from the Ramba Gneiss Dome (Liu et al., 2014), the Gyangze-Kangma area (Wang et al., 2016a, b) and the Lazi-Dingri area (Zeng et al., 2016) within the Tethyan Himalaya. Therefore, these two samples might represent magmatic rocks formed along the northern Indian passive margin, before the continental subduction of the Indian plate.

Did the ZBA also experience such magmatic event? If it did, one possible explanation would be that the ZBA in the NBC core was considerably influenced by the advection of the hot deep crust material, thus the older zircon grains might be totally recrystallized or homogenized and such record has been lost. Nevertheless, either the magmatic age in the PXA, or the existence of such Mesozoic event in the ZBA needs future investigation.

8. Conclusion

(a) Prograde, peak and retrograde metamorphic mineral assemblages of amphibolite from the core and outer part of the Namche Barwa Complex (NBC), southeastern Tibet, China, have been identified. Amphibolite samples record amphibolite-facies *P-T* conditions with clockwise metamorphic *P-T* paths. The metamorphic peak can be ascribed to medium *P/T* facies series.

(b) SIMS zircon U-Pb dating suggests that the Zhibai amphibolite, core of the NBC, experienced metamorphism from Oligocene to late Miocene (~30 Ma to ~10 Ma). The Paixiang amphibolite, outer part of the NBC, just records the late Miocene (~9 Ma) metamorphism.

(c) From Oligocene to late Miocene (30–10 Ma), semi-continuous advection of relatively hot materials from depth might have operated only in the NBC core, thus exhuming the Zhibai formation to a shallower level. Until late Miocene, rapid exhumation might have propagated from the core to the outer part of the NBC, and subsequently amalgamated as a coherent block after ~10 Ma.

(d) Inherited zircon core ages of ~80–90 Ma likely relate to magmatic events of the Indian Plate before its collision with the Eurasian Plate.

Acknowledgements

We sincerely thank Profs. Xian-Hua Li and Qiu-Li Li for guiding us in SIMS zircon U-Pb dating at the Institute of Geology and Geophysics, Chinese Academy of Sciences. We also thank Dr. Juan Wang, Mr. Jun-Xian Zhao and Mr. Jin-Fei Shi for their assistance in EPMA experiment, Miss Tian Zhou for her helpful discussion in processing SIMS data, and Dr. Richard Albert Roper for his linguistic assistance in revision for this manuscript. The quality of the original manuscript has been improved through reviews by two anonymous referees and the editorial review by Dr. Marco Scambelluri. This work was supported by the Key Research Program of Frontier Sciences from the Chinese Academy of Sciences (Grant No. QYZDJ-SSW-DQC036), the National Natural Science Foundation of China (41425010, 41430212), the China Geological Survey Project (12110115027101) and the State Scholarship Fund from China Scholarship Council (No. 201704910570).

Appendix A. Supplementary data

Supplementary data to this article can be found online at https://doi.org/10.1016/j.lithos.2018.10.002.

References

Bhadra, S., Bhattacharya, A., 2007. The barometer tremolite + tschermakite + 2 albite = 2 pargasite + 8 quartz: Constraints from experimental data at unit silica activity, with application to garnet-free natural assemblages. Am. Mineral. 92, 491–502.
Bonini, J.A., Baldwin, S.L., 1998. Mesozoic metamorphic and middle to late Tertiary magmatic events on Magdalena and Santa Margarita Islands, Baja California Sur, Mexico: Implications for the tectonic evolution of the Baja California continental borderland. Geol. Soc. Am. Bull. 110, 241–265.
Booth, A.L., Zeitler, P.K., Kidd, W.S.F., Wooden, J., Liu, Y.P., Idleman, B., Hren, M., Chamberlain, C.P., 2004. U-Pb zircon constraints on the tectonic evolution of southeastern Tibet, Namche Barwa area. Am. J. Sci. 304, 889–929.
Booth, A.L., Chamberlain, C.P., Kidd, W.S.F., Zeitler, P.K., 2009. Constraints on the metamorphic evolution of the eastern Himalayan syntaxis from geochronologic and petrologic studies of Namche Barwa. Geol. Soc. Am. Bull. 121, 385–407.
Burg, J.P., Davy, P., Nievergelt, P., Oberli, F., Seward, D., Diao, Z.Z., Meier, M., 1997. Exhumation during crustal folding in the Namche-Barwa syntaxis. Terra Nova 9, 53–56.
Burg, J.P., Nievergelt, P., Oberli, F., Seward, D., Davy, P., Maurin, J.C., Diao, Z.Z., Meier, M., 1998. The Namche Barwa syntaxis: evidence for exhumation related to compressional crustal folding. J. Asian Earth Sci. 16, 239–252.
Chen, H.-X., Wang, J., Wang, H., Wang, G.-D., Peng, T., Shi, Y.-H., Zhang, Q., Wu, C.-M., 2015. Metamorphism and geochronology of the Luoning metamorphic terrane, southern terminal of the Palaeoproterozoic Trans-North China Orogen, North China Craton. Precambrian Res. 264, 156–178.
Coleman, M.E., Hodges, K.V., 1998. Contrasting Oligocene and Miocene thermal histories from the hanging wall and footwall of the South Tibetan detachment in the central Himalaya from ^{40}Ar/^{39}Ar thermochronology, Marsyandi Valley, central Nepal. Tectonics 17, 726–740.
Corfu, F., Hanchar, J.M., Hoskin, P.W.O., Kinny, P., 2003. Atlas of zircon textures. Rev. Mineral. Geochem. 53, 469–500.
Cottle, J.M., Searle, M.P., Horstwood, M.S.A., Waters, D.J., 2009. Timing of midcrustal metamorphism, melting, and deformation in the Mount Everest region of southern Tibet revealed by U(-Th)-Pb Geochronology. J. Geol. 117, 643–664.
Dale, J., Holland, T., Powell, R., 2000. Hornblende-garnet-plagioclase thermobarometry: A natural assemblage calibration of the thermodynamics of hornblende. Contrib. Mineral. Petrol. 140, 353–362.
Ding, L., Zhong, D.L., 1999. Metamorphic characteristics and geotectonic implications of the high-pressure granulites from Namjagbarwa, eastern Tibet. Sci. China Ser. D Earth Sci. 42, 491–505.
Ding, L., Zhong, D.L., Yin, A., Kapp, P., Harrison, T.M., 2001. Cenozoic structural and metamorphic evolution of the eastern Himalayan syntaxis (Namche Barwa). Earth Planet. Sci. Lett. 192, 423–438.
Dupuy, C., Dostal, J., Bard, J.P., 1979. Trace element geochemistry of Paleozoic amphibolites from S. W. Spain. Mineral. Petrol. 26, 87–93.
Elueze, A.A., 1985. Petrochemical and Petrogenetic characteristics of Precambrian amphibolites of the Alawa district, northwest Nigeria. Chem. Geol. 48, 29–41.
Franceschelli, M., Puxeddu, M., Cruciani, G., Dini, A., Loi, M., 2005. Layered amphibolite sequence in NE Sardinia, Italy: remnant of a pre-Variscan mafic silicic layered intrusion? Contrib. Mineral. Petrol. 149, 164–180.
Gao, L., Zeng, L., Hou, K., Guo, C., Tang, S., Xie, K., Hu, G., Wang, L., 2013. Episodic crustal anatexis and the formation of Paiku composite leucogranitic pluton in the Malashan Gneiss Dome, Southern Tibet. Chin. Sci. Bull. 58, 3546–3563.
Geng, Q., Pan, G., Zheng, L., Chen, Z., Fisher, R.D., Sun, Z., Ou, C., Dong, H., Wang, X., Li, S., Lou, X., Fu, H., 2006. The Eastern Himalayan syntaxis: major tectonic domains, ophiolitic mélanges and geologic evolution. J. Asian Earth Sci. 27, 265–285.
Gerya, T.V., Perchuk, L.L., Triboulet, C., Audren, C., Sezko, A.I., 1997. Petrology of the Tumanshet Zonal Metamorphic Complex, Eastern Sayan. Petrology 5, 503–533.

de Gomes, C.B., Santini, P., Dutra, C.V., 1964. Petrochemistry of a Precambrian Amphibolite from the Jaraguá Area, São Paulo, Brazil. J. Geol. 72, 664–680.
Guilmette, C., Indares, A., Hebert, R., 2011. High-pressure anatectic paragneisses from the Namche Barwa, Eastern Himalayan Syntaxis: Textural evidence for partial melting, phase equilibria modeling and tectonic implications. Lithos 124, 66–81.
Guo, L., Zhang, H., Xu, W., 2008. U-Pb zircon ages of migmatite and granitic gneiss from Duoxiongla in eastern Himalayan syntaxis and their geological implications. Acta Petrol. Sin. 24, 421–429 (in Chinese with English abstract).
Holdaway, M.J., 2000. Application of new experimental and garnet Margules data to the garnet-biotite geothermometer. Am. Mineral. 85, 881–892.
Holdaway, M.J., Mukhopadhyay, B., 1993. A reevaluation of the stability relations of andalusite: Thermochemical data and phase diagram for the aluminum silicates. Am. Mineral. 78, 298–315.
Holland, T., Blundy, J., 1994. Non-ideal interactions in calcic amphiboles and their bearing on amphibole-plagioclase thermometry. Contrib. Mineral. Petrol. 116, 433–447.
Hoskin, P.W.O., Black, L.P., 2000. Metamorphic zircon formation by solid-state recrystallization of protolith igneous zircon. J. Metamorph. Geol. 18, 423–439.
Hoskin, P.W.O., Schaltegger, U., 2003. The composition of zircon and igneous and metamorphic petrogenesis. Rev. Mineral. Geochem. 53, 27–62.
Koons, P.O., Zeitler, P.K., Hallet, B., 2013. Tectonic aneurysms and mountain building. Treatise on Geomorphology. Elsevier, In, pp. 318–349.
Li, X.H., Liu, Y., Li, Q.L., Guo, C.H., Chamberlain, K.R., 2009. Precise determination of Phanerozoic zircon Pb/Pb age by multicollector SIMS without external standardization. Geochem. Geophys. Geosyst. 10, Q04010.
Li, Q.L., Li, X.H., Liu, Y., Tang, G.Q., Yang, J.H., Zhu, W.G., 2010. Precise U-Pb and Pb-Pb dating of Phanerozoic baddeleyite by SIMS with oxygen flooding technique. J. Anal. At. Spectrom. 25, 1107–1113.
Li, Q.L., Li, X.H., Wu, F.Y., Yin, Q.Z., Ye, H.M., Liu, Y., Tang, G.Q., Zhang, C.L., 2012. In-situ SIMS U-Pb dating of Phanerozoic apatite with low U and high common Pb. Gondwana Res. 21, 745–756.
Li, X.H., Tang, G.Q., Gong, B., Yang, Y.H., Hou, K.J., Hu, Z.C., Li, Q.L., Liu, Y., Li, W.X., 2013. Qinghu zircon: A working reference for microbeam analysis of U-Pb age and Hf and O isotopes. Chin. Sci. Bull. 58, 4647–4654.
Liu, F.L., Zhang, L.F., 2014. High-pressure granulites from Eastern Himalayan Syntaxis: *P-T* path, zircon U-Pb dating and geological implications. Acta Petrol. Sin. 30, 2808–2820 (in Chinese with English abstract).
Liu, Y., Zhong, D.L., 1997. Petrology of high-pressure granulites from the eastern Himalayan syntaxis. J. Metamorph. Geol. 15, 451–466.
Liu, Y., Siebel, W., Theye, T., Massonne, H.-J., 2011. Isotopic and structural constraints on the late Miocene to Pliocene evolution of the Namche Barwa area, eastern Himalayan syntaxis, SE Tibet. Gondwana Res. 19, 894–909.
Liu, Z.C., Wu, F.Y., Ji, W.Q., Wang, J.G., Liu, C.Z., 2014. Petrogenesis of the Ramba leucogranite in the Tethyan Himalaya and constraints on the channel flow model. Lithos 208–209, 118–136.
Lu, J.S., Wang, G.D., Wang, H., Chen, H.X., Wu, C.M., 2014. Palaeoproterozoic metamorphic evolution and geochronology of the Wugang block, southeastern terminal of the Trans-North China Orogen. Precambrian Res. 251, 197–211.
Ludwig, K.R., 2012. Isoplot 3.75-4.15 manual. A Geochronological Toolkit for Microsoft Excel. 4. Berkeley Geochronology Center Special Publication, pp. 1–70.
Ma, J., Wang, R.M., 1994. Reviews in garnet-clinopyroxene geothermometers and geobarometers with their application to granulite: The comparison of Miyun (Zunhua) and Xuanhua granulite forming condition. In: Qian, X., Wang, R.M. (Eds.), Geological Evolution of the Granulite Belt in North Part of North China Craton. Seismological Press, Beijing, pp. 71–78 (in Chinese).
Macfarlane, A.M., 1993. Chronology of tectonic events in the crystalline core of the Himalaya, Langtang National Park, central Nepal. Tectonics 12, 1004–1025.
Marroni, M., Frassi, C., Göncüoğlu, M.C., Di Vincenzo, G., Pandolfi, L., Rebay, G., Ellero, A., Ottria, G., 2014. Late Jurassic amphibolite-facies metamorphism in the Intra-Pontide Suture Zone (Turkey): an eastward extension of the Vardar Ocean from the Balkans into Anatolia? J. Geol. Soc. 171, 605–608.
Meng, J., Peng, T., Liu, J.H., Zhang, H.C.G., Wang, G.D., Lu, J.S., Chen, H.X., Wang, H.Y.C., Zhang, Q.W.L., Wu, C.M., 2017. Metamorphic evolution and SIMS zircon U-Pb geochronology of mafic granulite and amphibolite enclaves of the Pingyang trondhjemitic pluton, Fuping terrane, North China. Precambrian Res. 303, 75–90.
O'Brien, P.J., Rötzler, J., 2003. High-pressure granulites: formation, recovery of peak conditions and implications for tectonics. J. Metamorph. Geol. 21, 3–20.
Peng, T., Wang, H., Chen, H.X., Meng, J., Lu, J.S., Wang, G.D., Wu, C.M., 2014. Preliminary report on the metamorphic evolution of the Guanyingou amphibolites, Dunhuang Metamorphic Complex, NW China. Acta Petrol. Sin. 30, 503–511 (in Chinese with English abstract).
Reimann, C., Stumpfl, E.F., 1985. Paleozoic Amphibolites, Kreuzeck Mountains, Austria: Geochemical variations in the vicinity of mineralization. Mineral. Deposita 20, 69–75.
Rubatto, D., 2002. Zircon trace element geochemistry: partitioning with garnet and the link between U-Pb ages and metamorphism. Chem. Geol. 184, 123–138.
Schulz, B., Klemd, R., Brätz, H., 2006. Host rock compositional controls on zircon trace element signatures in metabasites from the Austroalpine basement. Geochim. Cosmochim. Acta 70, 697–710.
Searle, M.P., Waters, D.J., Rex, D.C., Wilson, R.N., 1992. Pressure, temperature and time constraints on Himalayan metamorphism from eastern Kashmir and western Zanskar. J. Geol. Soc. 149, 753–773.
Sláma, J., Košler, J., Condon, D.J., Crowley, J.L., Gerdes, A., Hanchar, J.M., Horstwood, M.S.A., Morris, G.A., Nasdala, L., Norberg, N., Schaltegger, U., Schoene, B., Tubrett, M.N., Whitehouse, M.J., 2008. Plešovice zircon – A new natural reference material for U-Pb and Hf isotopic microanalysis. Chem. Geol. 249, 1–35.
Spear, F.S., 1993. Metamorphic Phase Equilibria and Pressure-Temperature-Time Paths. Mineralogical Society of America, Washington, D.C., 799p.
Stacey, J.S., Kramers, J.D., 1975. Approximation of terrestrial lead isotope evolution by a two-stage model. Earth Planet. Sci. Lett. 26, 207–221.
Su, W., Zhang, M., Liu, X.H., Lin, J.F., Ye, K., Liu, X., 2012. Exact timing of granulite metamorphism in the Namche-Barwa, eastern Himalayan syntaxis: new constrains from SIMS U-Pb zircon age. Int. J. Earth Sci. 101, 239–252.
Sun, Z.M., Zheng, L.L., Geng, Q.R., Li, S., Liao, G.Y., Shi, W.L., Zhang, D., 2004. Genetic mechanisms and exhumation processes of the high-pressure granulites within the Eastern Himalayan syntaxis, Xizang. Sediment. Geol. Tethyan Geol. 24, 22–29 (in Chinese with English abstract).
Sun, Z.M., Dong, M., Liao, G.Y., Zheng, L.L., Geng, Q.R., Lou, X.Y., Li, S., Shi, W.L., Zhang, D., 2005. The granitic gneisses from the Namjagbarwa Group Complex within the eastern Himalayan syntaxis, Xizang. Sediment. Geol. Tethyan Geol. 25, 1–10 (in Chinese with English abstract).
Tian, Z.L., Zhang, Z.M., Dong, X., 2016. Metamorphism of high-*P* metagreywacke from the Eastern Himalayan syntaxis: phase equilibria and *P-T* path. J. Metamorph. Geol. 34, 697–718.
Tian, Z.L., Kang, D.Y., Mu, H.C., 2017. Metamorphic *P-T-t* path of garnet amphibolite from the Eastern Himalayan Syntaxis: Phase equilibria and zircon chronology. Acta Petrol. Sin. 33, 2467–2478 (in Chinese with English abstract).
Tsujimori, T., Liou, J.G., Ernst, W.G., Itaya, T., 2006. Triassic paragonite- and garnet-bearing epidote-amphibolite from the Hida Mountains, Japan. Gondwana Res. 9, 167–175.
Vijaya Kumar, K., Narsimha Reddy, M., Leelanandam, C., 2006. Dynamic melting of the Precambrian mantle: evidence from rare earth elements of the amphibolites from the Nellore-Khammam Schist Belt, South India. Contrib. Mineral. Petrol. 152, 243–256.
Wang, G.D., Wang, H., Chen, H.X., Lu, J.S., Wu, C.M., 2014a. Metamorphic evolution and zircon U-Pb geochronology of the Mts. Huashan amphibolites: Insights into the Palaeoproterozoic amalgamation of the North China Craton. Precambrian Res. 245, 100–114.
Wang, P., Scherler, D., Liu-Zeng, J., Mey, J., Avouac, J.-P., Zhang, Y., Shi, D., 2014b. Tectonic control of Yarlung Tsangpo Gorge revealed by a buried canyon in Southern Tibet. Science 346, 978–981.
Wang, Y.H., Zeng, L.S., Gao, L.E., Zhang, L.F., Hou, K.J., 2014c. Labradonian and Greenvillian orogenic events in the Namche Barwa Massif of the Himalayan orogenic belt. Acta Petrol. Sin. 30, 2241–2252 (in Chinese with English abstract).
Wang, H.Y.C., Chen, H.-X., Lu, J.-S., Wang, G.-D., Peng, T., Zhang, H.C.G., Yan, Q.-R., Hou, Q.-L., Zhang, Q., Wu, C.-M., 2016a. Metamorphic evolution and SIMS U-Pb geochronology of the Qingshigou area, Dunhuang block, NW China: Tectonic implications of the southernmost Central Asian orogenic belt. Lithosphere 8, 463–479.
Wang, Y.Y., Zeng, L.S., Gao, L.E., Zhao, L.H., Gao, J.H., Shang, Z., 2016b. Multiple Phases of Mafic Magmatism in Gyangze-Kangma Area: Implications for the Tectonic Evolution of Eastern Tethyan Himalaya. Acta Geol. Sin. 90, 129–130.
Wang, H.Y.C., Chen, H.-X., Zhang, Q.W.L., Shi, M.-Y., Yan, Q.-R., Hou, Q.-L., Zhang, Q., Kusky, T., Wu, C.-M., 2017a. Tectonic mélange records the Silurian-Devonian subduction-metamorphic process of the southern Dunhuang terrane, southernmost Central Asian Orogenic Belt. Geology 45, 427–430.
Wang, H.Y.C., Wang, J., Wang, G.-D., Lu, J.-S., Chen, H.-X., Peng, T., Zhang, H.C.G., Zhang, Q.W.L., Xiao, W.-J., Hou, Q.-L., Yan, Q.-R., Zhang, Q., Wu, C.-M., 2017b. Metamorphic evolution and geochronology of the Dunhuang orogenic belt in the Hongliuxia area, northwestern China. J. Asian Earth Sci. 135, 51–69.
Wang, H.Y.C., Zhang, Q.W.L., Lu, J.S., Chen, H.X., Liu, J.H., Zhang, H.C.G., Pham, V.T., Peng, T., Wu, C.M., 2018a. Metamorphic evolution and geochronology of tectonic mélange of the Dongbatu and Mogutai blocks, middle Dunhuang orogenic belt, northwestern China. Geosphere 14, 883–906.
Wang, H.Y.C., Zhang, Q.W.L., Chen, H.X., Liu, J.H., Zhang, H.C.G., Pham, V.T., Peng, T., Wu, C.M., 2018b. Paleozoic subduction of the southern Dunhuang Orogenic Belt, northwest China: metamorphism and geochronology of the Shuixiakou area. Geodin. Acta 30, 63–83.
Whitney, D.L., Evans, B.W., 2010. Abbreviations for names of rock-forming minerals. Am. Mineral. 95, 185–187.
Wiedenbeck, M., Alle, P., Corfu, F., Griffin, W.L., Meier, M., Oberli, F., Von Quadi, A., Roddick, J.C., Spigel, W., 1995. Three Natural Zircon Standards for U-Th-Pb, Lu-Hf, Trace Element and REE Analyses. Geostand. Geoanal. Res. 19, 1–23.
Wu, C.M., Zhang, J., Ren, L.D., 2004. Empirical garnet-biotite-plagioclase-quartz (GBPQ) geobarometry in medium- to high-grade metapelites. J. Petrol. 45, 1907–1921.
Xiao, L.L., Wang, G.D., Wang, H., Jiang, Z.S., Diwu, C., Wu, C.-M., 2013. Zircon U-Pb geochronology of the Zanhuang metamorphic complex: reappraisal of the Palaeoproterozoic amalgamation of the Trans-North China Orogen. Geol. Mag. 150, 756–764.
Xu, W.C., Zhang, H.F., Parrish, R., Harris, N., Guo, L., Yuan, H.L., 2010. Timing of granulite-facies metamorphism in the eastern Himalayan syntaxis and its tectonic implications. Tectonophysics 485, 231–244.
Xu, Z.Q., Ji, S.C., Cai, Z.H., Zeng, L.S., Geng, Q.R., Cao, H., 2012. Kinematics and dynamics of the Namche Barwa Syntaxis, eastern Himalaya: Constraints from deformation, fabrics and geochronology. Gondwana Res. 21, 19–36.
Xu, Z.Q., Wang, Q., Pecher, A., Liang, F., Qi, X.X., Cai, Z.H., Li, H.Q., Zeng, L.S., Cao, H., 2013. Orogen-parallel ductile extension and extrusion of the Greater Himalaya in the late Oligocene and Miocene. Tectonics 32, 191–215.
Yakymchuk, C., Kirkland, C.L., Clark, C., 2018. Th/U ratios in metamorphic zircon. J. Metamorph. Geol. 36, 715–737.
Yang, Y.N., Li, Q.L., Liu, Y., Tang, G.Q., Ling, X.X., Li, X.H., 2014. Zircon U-Pb dating by Secondary Ion Mass Spectrometry. Earth Sci. Front. 21, 81–92 (in Chinese with English abstract).
Zeitler, P.K., Meltzer, A.S., Koons, P.O., Craw, D., Hallet, B., Chamberlain, C.P., Kidd, W.S.F., Park, S.K., Seeber, L., Bishop, M., Shroder, J., 2001. Erosion, Himalayan Geodynamics, and the Geomorphology of Metamorphism. GSA Today 11, 4–9.

Zeitler, P.K., Meltzer, A.S., Brown, L., Kidd, W.S.F., Lim, C., Enkelmann, E., 2014. Tectonics and topographic evolution of Namche Barwa and the easternmost Lhasa block, Tibet. In: Nie, J., Horton, B.K., Hoke, G.D. (Eds.), Toward an Improved Understanding of Uplift Mechanisms and the Elevation History of the Tibetan Plateau. Geological Society of America Special Paper 507, pp. 23–58.

Zeng, L., Gao, L.-E., Dong, C., Tang, S., 2012. High-pressure melting of metapelite and the formation of Ca-rich granitic melts in the Namche Barwa Massif, southern Tibet. Gondwana Res. 21, 138–151.

Zeng, L., Wang, Y.H., Gao, L.-E., Wang, Y.Y., 2016. Elusive Cenozoic metamorphism in mafic dike swarms within the Tethyan Himalaya, southern Tibet. Acta Geol. Sin. Engl. Ed. 90 (Supp. 1), 86–87.

Zhang, Z.M., Wang, J., Zhao, G., Shi, C., 2008. Geochronology and Precambrian tectonic evolution of the Namche Barwa complex from the eastern Himalayan syntaxis, Tibet. Acta Petrol. Sin. 24, 1477–1487 (in Chinese with English abstract).

Zhang, Z.M., Zhao, G.C., Santosh, M., Wang, J.L., Dong, X., Liou, J.G., 2010. Two stages of granulite facies metamorphism in the eastern Himalayan syntaxis, south Tibet: petrology, zircon geochronology and implications for the subduction of Neo-Tethys and the Indian continent beneath Asia. J. Metamorph. Geol. 28, 719–733.

Zhang, Z.M., Dong, X., Santosh, M., Liu, F., Wang, W., Yiu, F., He, Z.Y., Shen, K., 2012. Petrology and geochronology of the Namche Barwa Complex in the eastern Himalayan syntaxis, Tibet: Constraints on the origin and evolution of the north-eastern margin of the Indian Craton. Gondwana Res. 21, 123–137.

Zhang, Z.M., Xiang, H., Dong, X., Ding, H.X., He, Z.Y., 2015. Long-lived high-temperature granulite-facies metamorphism in the Eastern Himalayan orogen, south Tibet. Lithos 212–215, 1–15.

Zheng, X.L., Chang, C.F., 1979. Cenozoic multistage magmatism and tectonic significance of the southeastern segment of the Gangdese belt, Tibetan Plateau. Sci. Geol. Sin. 116–126 (in Chinese).

Zhong, D.L., Ding, L., 1995. The find of high-pressure granulite in Namche Barwa, Tibet. Chin. Sci. Bull. 40, 1343 (in Chinese).